PERGAMON

International Journal of Rock Mechanics & Mining Sciences 39 (2002) 185–216

International Journal of
Rock Mechanics
and Mining Sciences

www.elsevier.com/locate/ijrmms

Some new Q-value correlations to assist in site characterisation and tunnel design

N. Barton*

Nick Barton and Associates, Fjordveien 65c, 1363 Høvik, Norway

Accepted 5 February 2002

Abstract

The rock mass quality Q-value was originally developed to assist in the empirical design of tunnel and cavern reinforcement and support, but it has been used for several other tasks in rock engineering in recent years. This paper explores the application of Q and its six component parameters, for prediction, correlation and extrapolation of site investigation data, and for obtaining first estimates of some input data for both jointed distinct element and continuum-approximation modelling. Parameters explored here include P-wave velocity, static modulus of deformation, support pressure, tunnel deformation, Lugeon-value, and the possible cohesive and frictional strength of rock masses, undisturbed, or as affected by underground excavation. The effect of depth or stress level, and anisotropic strength, structure and stress are each addressed, and practical solutions suggested. The paper concludes with an evaluation of the potential improvements in rock mass properties and reduced support needs that can be expected from state-of-the-art pre-injection with fine, cementicious multi-grouts, based on measurements of permeability tensor principal value rotations and reductions, caused by grout penetration of the least favourable joint sets. Several slightly improved Q-parameter ratings form the basis of the predicted improvements in general rock mass properties that can be achieved by pre-grouting. © 2002 Elsevier Science Ltd. All rights reserved.

1. Introduction

The traditional application of the six-parameter Q-value in rock engineering is for selecting suitable combinations of shotcrete and rock bolts for rock mass reinforcement and support. This is specifically the permanent 'lining' estimation for tunnels or caverns in rock, and mainly for civil engineering projects.

The Q-value is estimated from the following expression:

$$Q = \frac{\mathrm{RQD}}{J_n} \times \frac{J_r}{J_a} \times \frac{J_w}{\mathrm{SRF}} \quad (1)$$

where RQD is the % of competent drill-core sticks >100 mm in length [1] in a selected domain, J_n is the rating for the number of joint sets (9 for 3 sets, 4 for 2 sets, etc.) in the same domain, J_r is the rating for the roughness of the least favourable of these joint sets or filled discontinuities, J_a is the rating for the degree of alteration or clay filling of the least favourable joint set or filled discontinuity, J_w is the rating for the water inflow and pressure effects, which may cause outwash of discontinuity infillings, and SRF is the rating for faulting, for strength/stress ratios in hard massive rocks, for squeezing or for swelling.

The above ratings, and some important new footnotes, are given in full in Appendix A. The three quotients appearing in Eq. (1) have the following general or specific role:

RQD/J_n is the relative block size (useful for distinguishing massive, rock-burst-prone rock), J_r/J_a is the relative frictional strength (of the least favourable joint set or filled discontinuity), and J_w/SRF is the relative effect of water, faulting, strength/stress ratio, squeezing or swelling (an 'active stress' term). An alternative combination of these three quotients in two groups only, has been found to give fundamental properties for describing the shear strength of rock masses. This aspect will be described towards the end of the paper, after exploring a number of simple correlations between engineering parameters and Q-values, the latter normalised to the form Q_c, for improved sensitivity to widely varying uniaxial compression strengths.

*Tel.: +47-67-53-15-06.
E-mail address: nickrbarton@hotmail.com (N. Barton).

1365-1609/02/$ - see front matter © 2002 Elsevier Science Ltd. All rights reserved.
PII: S1365-1609(02)00011-4

Nomenclature

Δ	deformation measured in tunnel or cavern (related to dimension of excavation span)
Δ_v	vertical component of deformation
Δ_h	horizontal component of deformation (assume half of horizontal convergence)
λ	joint spacing (m^{-1})
γ	rock mass density (t/m^3)
σ_c	uniaxial compression strength (MPa)
$SIGMA_{cm}$	rock mass compression strength based on compression failure of the intact portions (only an estimate since no hard data)
$SIGMA_{tm}$	rock mass compression strength based on tensile failure of the intact portions (only an estimate since no hard data)
σ_h	horizontal component of stress (relevant to problem considered)
σ_r	radial stress around an excavation in rock
σ_v	vertical principal stress
ϕ	friction angle of joint or discontinuity (peak or post peak, relevant to the conditions)
'ϕ'	friction angle of rock mass (degrees, estimated from RMR)
ϕ_r	residual friction angle of a joint
3DEC	three-dimensional distinct element code for modelling jointed rock masses
B	systematically spaced steel rock bolt
BB	Barton–Bandis constitutive model for rock joints, used with UDEC
'c'	cohesion of rock mass (MPa, estimated from RMR)
CC	cohesive component of rock mass strength (MPa, given by RQD, J_n, SRF and $\sigma_c/100$)
CCA	cast concrete arches
E_{dyn}	dynamic modulus of deformation
E_{mass}	static modulus of deformation
E	average physical aperture of a joint
e	hydraulic aperture
EDZ	excavation disturbed zone
ESR	excavation support ratio (see Q-support chart)
FC	frictional component of rock mass strength (degrees, given by J_r, J_a and J_w)
FEM	finite element method of numerical modelling
FLAC	two-dimensional continuum code for modelling small or large deformations in rock or soil
$FLAC^{3D}$	three-dimensional continuum code for modelling small or large deformations in rock or soil
FRP	fibre reinforced plastic bolts
GSI	geological strength index
i	with + or − implies dilation or contraction when loaded in shear
I_{50}	point load index for 50 mm size samples (high ratios of σ_c/I_{50} give $SIGMA_{cm} > SIGMA_{tm}$)
IPT	Institute of Technological Research (Sao Paulo)
J_a	rating for joint alteration, discontinuity filling (of least favourable set or discontinuity)
JCS	joint wall compression strength
J_n	rating for number of joint sets
J_r	rating for joint surface roughness (of least favourable set or discontinuity)
JRC	joint roughness coefficient
J_w	rating for water softening, inflow and pressure effects
K	permeability (units m/s)
K_{int}	intermediate principal permeability
K_{max}	maximum principal permeability
K_{min}	minimum principal permeability
K_0	ratio of σ_h/σ_v
L	Lugeon unit of water injection (l/min/m/1 MPa) ($\approx 10^{-7}$ m/s in units of permeability)
MPBX	multiple position borehole extensometer
NATM	new Austrian tunnelling method for weaker rock [B + S(mr) or S(fr), monitoring, and final CCA lining]
NGI	Norwegian Geotechnical Institute (Oslo)
NMT	Norwegian method of tunnelling for stronger rock (Q-classification, and final B + Sfr)

P_r	support pressure—estimate of required radial capacity of support, e.g. B + S(fr)
Q	rock mass quality rating (range 10^{-3} to 10^{3})
Q_c	rock mass quality rating (Q, or Q_0, normalised by $\sigma_c/100$)
Q_0	Q calculated with RQD_0 oriented in the loading or measurement direction
Q_{seis}	seismic quality factor—the inverse of attenuation (used by geophysicists, normally with the P- and S-wave components 'Q_p' and 'Q_s', and the coda wave 'Q_c')
Q_t	rock mass quality rating (Q, or Q_0, normalised by $I_{50}/4$) (should be used for strongly anisotropic rock types)
RMi	rock mass index
RMR	rock mass rating
RQD	rock quality designation
RQD_0	RQD oriented in the loading or measurement direction (in the Q_{TBM} model it is in the tunnelling direction)
RRS	steel rib-reinforced-shotcrete arches
S(fr)	steel fibre reinforced sprayed concrete
S(mr)	steel mesh reinforced shotcrete
$SIGMA_{cm}$	rock mass compression strength based on compression failure of the intact portions (only an estimate since no hard data)
$SIGMA_{tm}$	rock mass compression strength based on tensile failure of the intact portions (only an estimate since no hard data)
SKB	Swedish Nuclear Fuel Co. (Stockholm)
SPAN or HEIGHT	are the horizontal or vertical dimensions of a tunnel or cavern
SRF	rating for faulting, strength/stress ratios, squeezing, swelling
TBM	tunnel boring machine
UDEC	universal distinct element code, for modelling a two-dimensional, 1 m thick slice of the rock mass
V_p	P-wave seismic velocity (km/s)
V_s	S-wave seismic velocity (km/s)

The first two quotients RQD/J_n and J_r/J_a are often used in a stope design method in the mining industry, but their representation of 'relative block size' and 'inter-block shear resistance' are not sufficient descriptions of the degree of instability. The possible presence of water and of faults or adverse stress (both too high or too low) also needs to be included, at least when these are present [2]. The original difficulty of matching support needs when using only four or five of the original parameters were used, is also recalled.

The development of the Q-system in the early 1970s [3], followed a period of pre-occupation with the shear strength of rock joints and of clay-filled discontinuities. Perhaps for this reason the three rock-to-rock contact categories of J_r and J_a (seen in Tables A3 and A4 in the appendix) seem to ensure a sensible weighting of this most important of rock mass parameters, namely the shear resistance of the least favourable joints or filled discontinuities. The potentially dilatant character of many joints, and the often contractile character of filled discontinuities, is captured in the ratio J_r/J_a, which resembles a dilatant or contractile coefficient of friction.

The original 212 case records of tunnels and caverns from 50 different rock types [4], were each analysed several times, during the six month period needed for development of the Q-parameters. This was in order to calibrate and re-calibrate the ratings, to match the final Q-value with the support and reinforcement needs. Parameter ratings needed successive fine-tuning, to bring the 'all-encompassing' Q-value into reasonable correspondence with the necessary level of rock reinforcement (fully grouted rock bolts) and with the necessary level of shotcrete or concrete support for the excavated perimeters (arch, walls and sometimes the invert as well).

The early set of 212 case records were derived from a period (approximately 1960–1973) when plain shotcrete (S), or steel-mesh reinforced shotcrete, termed S(mr), or cast concrete arches, termed CCA, were used for tunnel and cavern support, together with various types of rock bolts. Since the 1993 update of support recommendations with 1050 new case records [5], the superficial support has undergone a revolutionary improvement to mostly steel-fibre reinforced sprayed concrete, termed S(fr) in place of S(mr). Cured cube strength qualities of 35–45 MPa or more are now readily available with wet process, microsilica-bearing, and non-alkali accelerated sprayed concrete. The updated Q-support chart is shown in Fig. 1. The new case records were collected over a period of several years by Grimstad

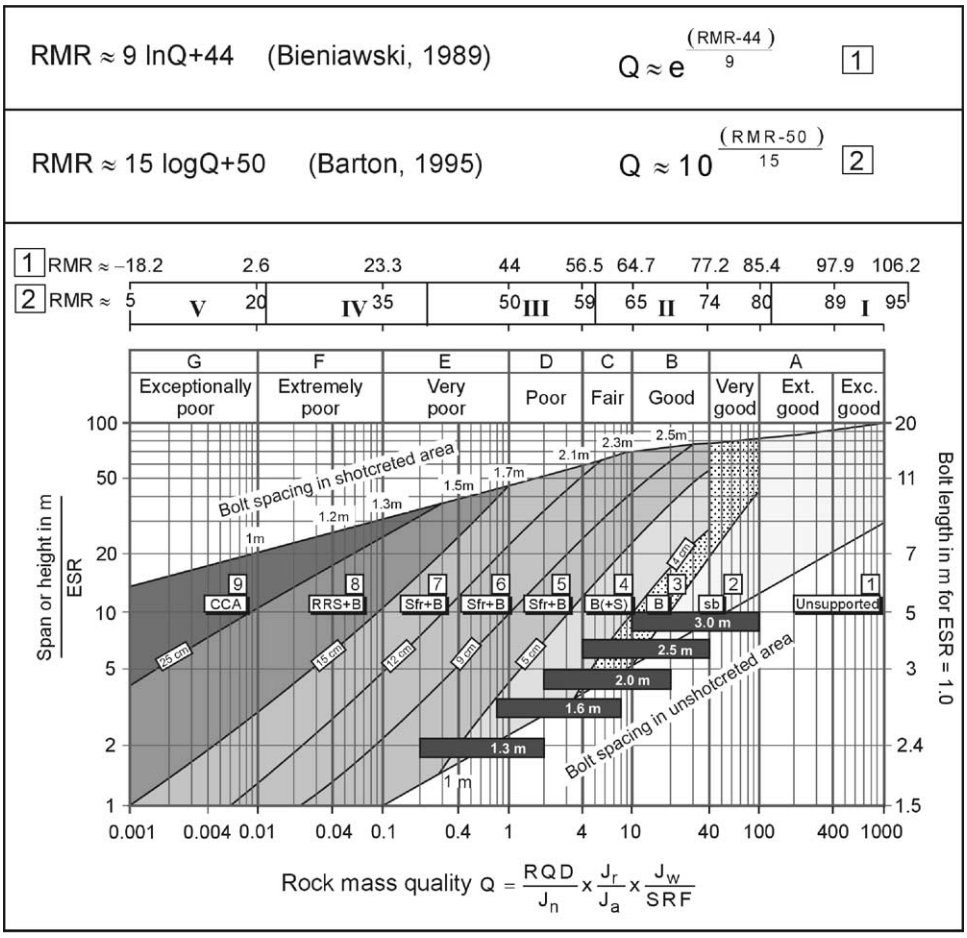

Fig. 1. The 1993 updated *Q*-support chart for selecting permanent B + S(fr) reinforcement and support for tunnels and caverns in rock [5]. The black, highlighted areas show where estimated *Q*-values and stability are superior in TBM tunnels compared to drill-and-blast tunnels. This means 'no support' penetrates further.

of NGI, from tunnels that were *not* designed by the *Q*-system [5].

Despite the significant number of new case records, it was hardly found necessary to make any changes to the 20-year old *Q*-parameter ratings. Just three of the strength/stress SRF ratings were increased to bring massive (high RQD/J_n) rock masses under extremely high stress sufficiently far 'to the left' in the support chart to receive appropriate quantities of systematic bolting (B), and S(fr). Previously, such cases were supported in an entirely different way, and were treated in a footnote in [3], prior to the development of S(fr) at the end of the 1970s.

2. Numerical modelling needs

During the period leading up to the development of the updated support methods detailed in Fig. 1, the writer was involved in an increasing number of projects that required numerical verification of the empirical tunnel and cavern designs. Motorway tunnels in Norway, Hong Kong and Japan, caverns in Israel and England, and the 62 m span Gjøvik cavern in Norway [6], figured prominently in an identification of the obvious need for improved correlations between rock mass classification, general site investigation data, and the final input data for distinct element (i.e. jointed) two-dimensional (UDEC-BB) and three-dimensional (3DEC) models developed principally by Cundall.

Although the dominant joint sets were generally modelled using the JRC, JCS and ϕ_r index parameters and the Barton–Bandis constitutive model, or using derived Mohr–Coulomb parameters for 3DEC, there was a need for a measure of rock mass deformation modulus that accounted for the normally rather small scale (a few m^3) of jointed rock that occurred between the more dominant but widely spaced joints. The former would be responsible for a reduced RQD if drilled through, and would normally be the subject of plate load tests, beneath which there may often be few of the dominant joints that have to be represented in say, a 50×100 m, 2-D numerical simulation.

A graphic example of this 'scale effect' is shown in Fig. 2. While the logged values of RQD and J_n must include all scales of the rock mass structure, every detail cannot be modelled discretely, and one is forced to include in a distinct element model only the joint sets assumed to have most influence on, for example, the stability of the modelled tunnels or cavern. A representative value for the modulus of deformation of a limited rock mass volume is still required, onto which will be superimposed the larger scale 'REV' (representative elementary volume) response of the rock mass as a whole, in which a fault might also be modelled, if close enough to the excavation under investigation. The stiffness of the fully consolidated major joint sets is likely to modify the assumed modulus of deformation, and may also give anisotropic deformability, i.e. details not usually captured in continuum modelling.

The less dominant jointing is reflected in a reduced Q-value, and in a reduced P-wave velocity (V_p) and static modulus of deformation. We will define the latter as E_{mass} in this paper, to distinguish it from Young's modulus and from the physical joint aperture (E), where $E > e$, the smooth parallel plate hydraulic aperture used in the cubic law. This inequality is due to effects of joint roughness JRC, and flow tortuosity around areas of rock-to-rock contact [7] which will be addressed when discussing grouting.

3. Correlation of Q with V_p

In view of the importance of the site investigation phase that precedes preliminary design, and which gives indications of the need for additional hydrogeologic information, we will start this exploration of Q-correlations with an investigation of seismic velocity. Some recent examples of available seismic techniques have been given in this Journal (vol. 38, No. 6, Sept 2001) and will be referred to shortly.

If shallow seismic refraction data, or deeper cross-hole tomography, or VSP, can be extrapolated by means of one or more correlations between Q and V_p, then some of the uncertainties in tunnelling or cavern design could be removed. However, there are several potential pitfalls, which have led some to assume that seismic data may be unreliable. The truth is probably that the physics have not been understood.

Based on data from hard rock tunnelling projects in several countries, including the 62 m span Gjøvik cavern in Norway where NGI performed seismic tomography and core logging, a preliminary hard rock correlation between Q and V_p was suggested [8]:

$$V_p \approx 3.5 + \log Q \quad (2)$$

where V_p is in units of km/s. (Note: all logarithmic terms are $\log_{10}$ in this paper.)

Important clues supporting this relation were subsequently discovered from extensive earlier work by Sjøgren and co-workers [9], who had presented V_p, RQD and joint frequency ($\lambda\,m^{-1}$) data from 120 km of seismic refraction profiles and 2.8 km of adjacent core data. Fig. 3a shows the mean trends of this data (with some slight extrapolations by the writer). Along the x-axis of both figures is appended the simple $V_p - Q$ relation given by Eq. (2).

The above relation between V_p and Q was subsequently generalised to include rock that could be weaker or even stronger than the assumed 'hard' rock. Normalisation of the Q-value was tested, using 100 MPa as the hard rock norm. For improving correlation to

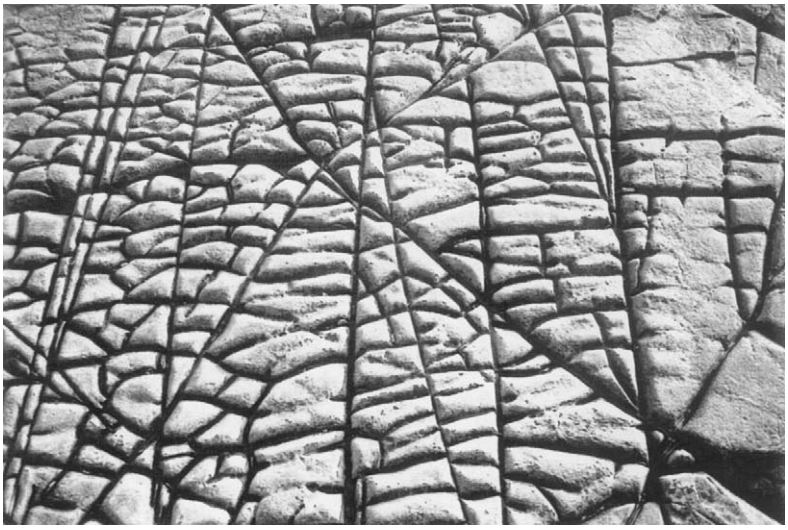

Fig. 2. An illustrative 'textbook example' of dominant joints (strong continuity, low JRC, JCS and ϕ_r) requiring distinct element modelling, and the less dominant 'back-ground' jointing (higher JRC, JCS and ϕ_r) which will nevertheless be represented in RQD and J_n and in a reduced deformation modulus and seismic velocity. Kimmeridge Bay, South Coast, England [writer].

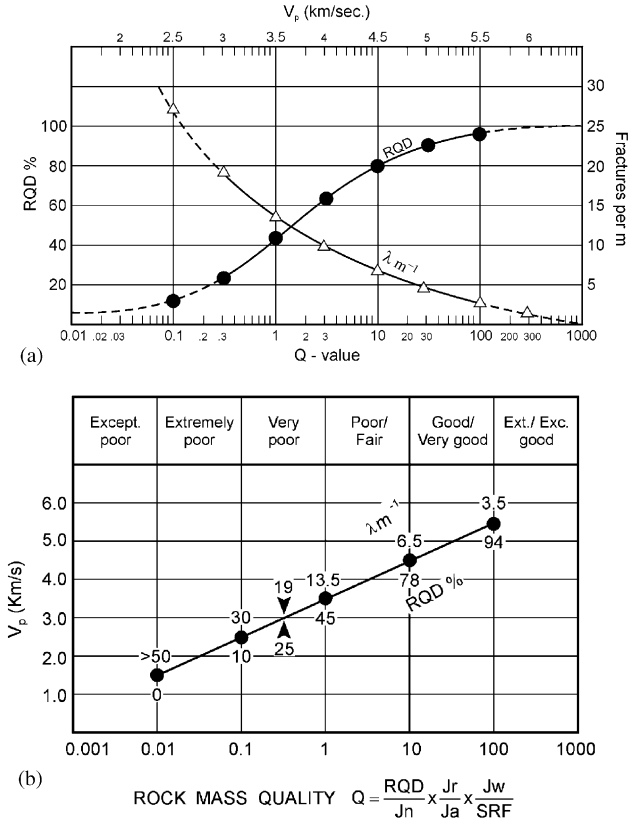

Fig. 3. (a,b) Mean correlations of V_p, RQD and $\gamma\,m^{-1}$ for shallow refraction seismic at hard rock sites from [9], with the writer's extrapolations and appended Q-scales, also for shallow, hard rock sites, based on [8].

engineering parameters, as described in this paper, Q_c was finally defined as

$$Q_c = Q \times \frac{\sigma_c}{100} \tag{3}$$

which means that σ_c, the uniaxial compressive strength is contributing to the description of quality, even when the strength/stress ratio is insufficient to 'mobilise' an SRF-value >1.0, as in the normal Q-parameter classification for tunnel support selection, which remains unaffected by the Q_c term.

The uniaxial compressive strength, which is easy to measure or estimate, correlates strongly with Young's modulus, and therefore figures quite strongly in improving the estimates of velocities (and deformation moduli). Uniaxial compressive strength also tends to correlate with porosity and density, both of which correlate independently with seismic velocity. The improved $Q-V_p$ correlation is

$$V_p \approx 3.5 + \log Q_c \tag{4}$$

This equation forms the central core of the integrated V_p-Q (and modulus) relationship shown in Fig. 4. Trial and error fitting of a depth correction (a +ve correction) and a porosity correction (a −ve correction) was performed using both low velocity and high velocity rocks, and those with significant or negligible porosities. Channel Tunnel chalk marl, various chalks from Israel [10], sandstones and shales from China and Japan, granites and gneisses from Norway and Hong Kong, and ignimbrites and tuffs from England and Hong Kong were among the most prominent sets of seismic data where Q-values had also been logged by the writer, and by others.

4. Effect of depth or stress on V_p

Increased depth or stress tends to increase V_p for any given RQD, λ (m^{-1}), or Q-value. However, when the rock is very weak 'seismic closure' of the joints will occur at shallow depth, while stronger rocks will require greater depths to reach 'stable' velocities [12]. Deformable features like clay-bearing faults may be so compacted at many hundreds of meters depth that they may be 'invisible' to seismic velocity tomography carried out ahead of a struggling TBM (viz. Pont Ventoux in Italy). Months of delay when tunnelling, where V_p is supposedly in excess of 4.5 km/s, obviously requires a depth correction, as shown in Fig. 4.

Occasionally, a set of velocity data may demonstrate the depth or stress effect, without the nagging doubt about the actual effect of the improved qualities that may accompany the depth increase. Important data from the Chinnor Tunnel in Lower Chalk [13] are reproduced in Fig. 5. The moderately increased overburden produced an expected velocity increase, yet in this case the joint frequency actually *increased* with depth. Stress increase alone apparently caused the increase in V_p.

Some of the seismic tomography and depth-effects observed at the Gjøvik cavern site [6] are reproduced in Fig. 6. Despite no systematic increase in RQD or decrease in λ (m^{-1}), or increase in Q-value in the first 60 m, the P-wave velocity increased by almost 2 km/s adjacent to one of the vertical boreholes. The key to understanding this strong depth effect is that both the minor, and especially the major horizontal stress increased by several MPa over the same depth interval. The predominant ($J_r = 3$) joint sets in the 60–90 MPa tectonized gneiss were of the steeply dipping, conjugate variety. These were rapidly becoming acoustically 'closed' by the high horizontal stresses.

Having established a case for a depth (and porosity) correction to V_p, as shown in Fig. 4, two examples will be given to illustrate the method:

Assume the following: Q-value = 10 (core from 250 m depth); $\sigma_c = 10$ MPa; porosity = 11%; $Q_c = 10 \times 10/100 = 1.0$.

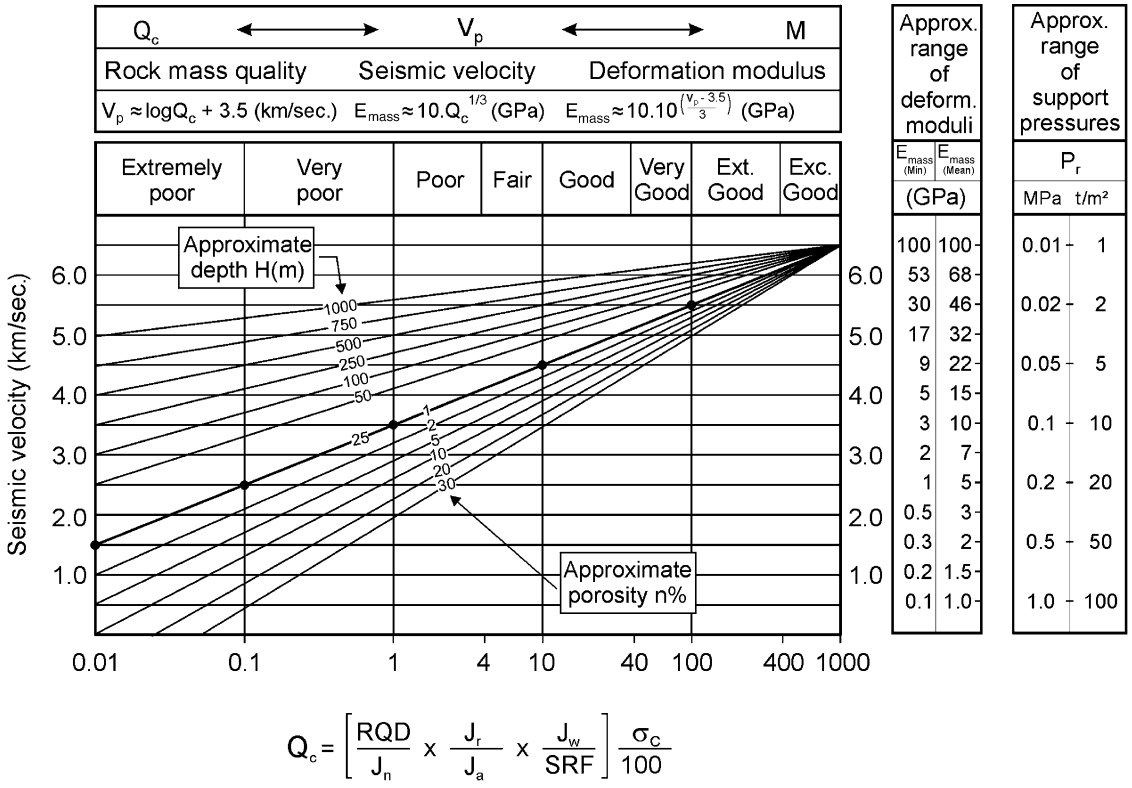

Fig. 4. An integration of V_p, Q, σ_c, depth, porosity and static deformation modulus E_{mass}, which was developed stage by stage, by trial-and-error fitting to field data [11].

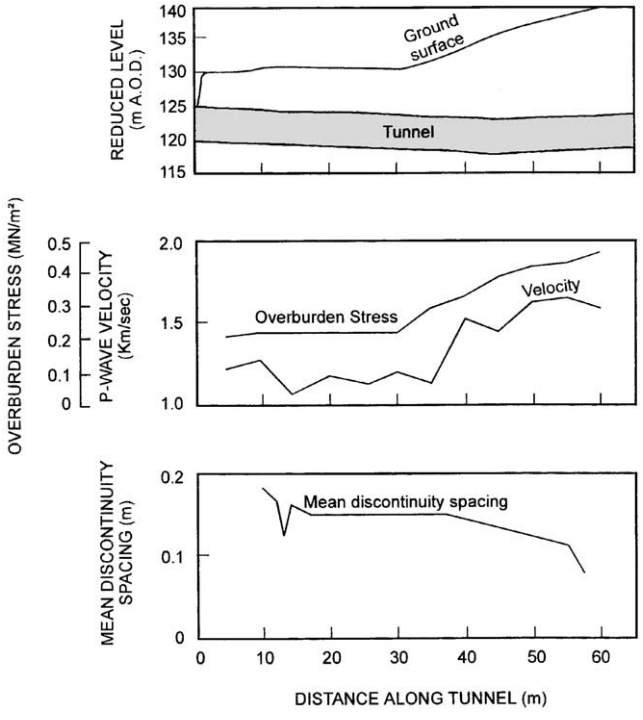

Fig. 5. Seismic velocity measurements in the Lower Chalk at the Chinnor Tunnel in Oxfordshire, England. V_p increases with depth despite *increased* joint frequency [13,14].

The 250 m depth line (Fig. 4) shows $V_p = 4.7$ km/s when $Q_c = 1.0$ (this is a potential 1.2 km/s increase above the Eq. (4) reference line). Porosity of 11% requires a reduction of about 0.9 km/s for this same Q_c. The predicted down-hole velocity would therefore be $3.5 + 1.2 - 0.9 = 3.8$ km/s. The procedure needs to be reversed when estimating a Q-value from a down-hole (or *stressed* velocity).

For example, at 500 m depth, a stressed V_p of 5.0 km/s would imply a Q_c of 1.0 if there was negligible porosity (nominal 1%). The Q-value should be about equal to $Q_c \times 100/(\sigma_c)$ by reversing Eq. (3). In other words $Q = 4$ if $\sigma_c = 25$ MPa. The estimate of Q_c climbs higher than 1.0 if there is porosity > 1.0. If the porosity was 8%, Q_c could be as high as 10, based on the balance of velocities (i.e. $4.5 + 1.0 - 0.5 = 5.0$ km/s). The Q-value might then be as high as $10 \times 100/25 = 40$.

At SKBs Äspö ZEDEX (zone of excavation disturbance experiment in Sweden), stressed velocities of about 5.9–6.2 km/s were recorded by Cosma and colleagues [15,16], using numerous, long radial holes drilled from the selected sections of the drill-and-blast and TBM tunnels. This cross-hole tomography was performed at nearly 450 m depth in diorites and granites ranging in strength from about 170–260 MPa. The

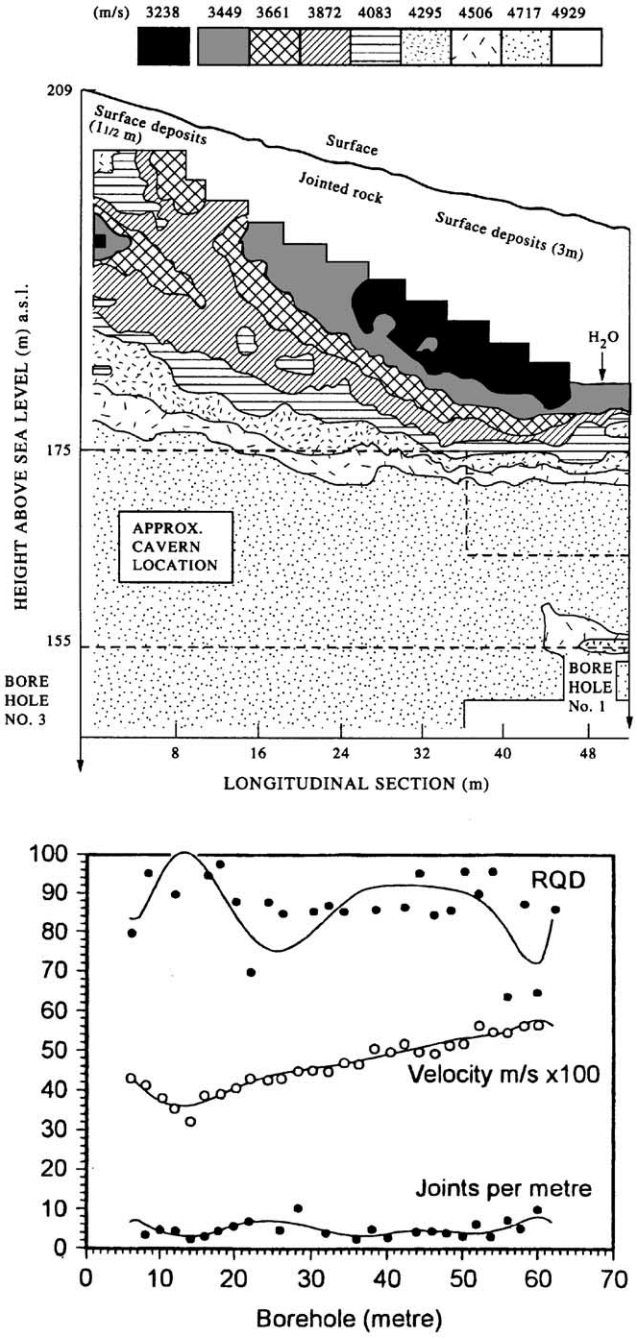

Fig. 6. A seismic tomography result for the jointed gneiss at the Gjøvik Cavern site in Norway. V_p increases with depth despite the fairly stable RQD, $\gamma\,m^{-1}$ and Q-values over the same depth range. The mean Q-value was about 10, see [6].

principal stresses were approximately 32, 17 and 10 MPa. In this case we have to consider a stress or depth correction, and the positive influence of the hard, non-porous rocks. Inspection of Fig. 4 shows that the equation of the 500 m depth line is given by

$$V_p = 5.0 + 0.5\log Q_c \quad (5)$$

This 500 m line could represent the mean of the two principal stresses of 10 and 17 MPa. If Q_c was as high as 60–250, the measured velocities of 5.9–6.2 km/s would be 'explained'. However, using the σ_c range of 170–260 MPa, and the Q_c normalisation, a narrower Q-value range of 35–96 is predicted. The second of these values is perhaps twice as high as logged, while the first value is realistic.

When logging to *characterise* a deep site, as opposed to Q-logging for empirical tunnel design, one should use the SRF value of 0.5, which is appropriate to 'high stress, tight structure', as shown in Table A6 (section b) in the appendix, and in relevant footnotes. This will tend to give a higher Q-value (a virgin Q-value) unassociated with the stress changes caused by excavation, which may cause the mobilisation of a higher SRF value that is appropriate for empirical selection of support in a stress-fractured, but otherwise massive rock mass.

The above examples are given in order to show the importance of *not* assuming that seismic measurements are giving 'misleading' results. Such was the case recently in Norway, in a dry sub-sea tunnel, acted on by a significant depth of sea water 'cover', where high velocities measured from the seabed, gave a misleading impression of good quality rock masses, giving the contractor reason to regret the low bid price. If the rock mass had been saturated, a much lower velocity would have been recorded, giving a more correct impression of the actual bad conditions.

In the same way, one should also be open to the possibility that the major principal stress of 32 MPa at the Äspö ZEDEX site, may be causing a physically explainable additional closure of one of the two or more joint sets, giving for example, an 'equivalent depth' of at least 1000 m in Fig. 4. With $V_p = 6.2$ km/s, $Q_c = 100$ and $\sigma_c = 260$ MPa, the predicted Q-value of about 38 is just where it should be on the 10^{-3} to 10^{+3} Q-scale; typical of many logged values.

5. Correlation of Q with E_{mass}

There have been several stages in the development of empirical models that relate E_{mass}, the static modulus of deformation modulus, and the rock mass quality terms, such as RMR which arrived first in 1973, and Q which followed independently a year later. Here, we will concentrate mostly on Q-value relations, the first of which for mean values of modulus was

$$E_{mass} = 25\log Q \quad (6)$$

Naturally, this 1980 relation [17] was only applicable to $Q > 1$ and generally hard rocks. It served very well for instance in UDEC-BB distinct element modelling of the Gjøvik cavern [18], but already a need for a depth or stress correction was recognised, and three values of

modulus were used, increasing from 20 GPa in the near-surface to 40 GPa at depth.

An earlier 1978 equation relating E_{mass} and RMR [19] was also designed for only the upper end of the quality scale

$$E_{mass} = 2RMR - 100 \quad (7)$$

and was only applicable to RMR > 50. The latter is shown in Fig. 7, to contrast with the subsequent Portuguese improvement and generalisation [20]:

$$E_{mass} = 10^{(RMR-10)/40} \quad (8)$$

and the later Q_c-based improvement, using the normalisation of the Q-value given by Eq. (3) [11,21]:

$$E_{mass} = 10Q_c^{1/3} \quad (9)$$

The values of E_{mass} tabulated on the right-hand side of Fig. 4 (E_{mass} mean) are derived from Eq. (9). Note their strong non-linearity compared to the linear V_p scale. Note also the adjacent table of E_{mass} (min) values that were given specifically to account for 'inexplicably' low values of modulus [11]. In fact the latter are due to the effects of excessive loosening or EDZ (excavation disturbed zone). Low moduli and low velocities in relation to assumed (i.e. logged) rock mass qualities can be quantitatively explained by the excessive development of joint 'porosity' or slight voidage, which affects two of the three potential velocity components (through air and/or water), and also gives unexpectedly lower normal stiffness due to the non-linearity and hysteretic behaviour of slightly sheared and/or opened joints [12,22].

The two curves shown in Fig. 7 are seen to coalesce for Q-values <1 and RMR <50, if one applies the conversion [11] between Q and RMR shown in Fig. 7, which gives by elimination of RMR:

$$E_{mass} = 10^{(15\log Q+40)/40} \quad (10)$$

For example, when $Q = 0.1$ or 0.01 (and log Q is equal to -1 or -2) RMR is predicted to be 35 or 20, respectively, which will be seen by inspection to give the same coefficients in Eqs (8) and (10), giving equal predictions of $E_{mass} = 4.2$ and 1.8 GPa, respectively.

For Q-values above 1.0 and RMR above 50, the coefficients diverge, and Eq. (9) gives a more conservative value of modulus, *unless* $\sigma_c > 100$ MPa. Conversely, if σ_c is <100 MPa, as it usually will be when rock is of very poor quality, Eq. (9) will then give a predicted modulus lower than Eq. (8). This in fact is necessary, as an assumed minimum RMR of about 10 will give a predicted modulus no lower than 1.0 GPa, although use of the adverse (and negative) orientation term could *theoretically* give negative RMR, though in [23], the lowest class is referred to as RMR<20, i.e. presumably not so close to zero.

Pushing the limits of Eq. (9), we could consider $Q = 0.001$ (exceptionally poor quality) and the limiting range for very weak rocks of $\sigma_c = 0.25-1.0$ MPa. An extreme lower bound Q_c range of 0.0000025–0.00001 (from Eq. (3)) gives a predicted minimum range for 'rock masses' of $E_{mass} = 0.14-0.22$ GPa. This is close to the lowest values measured or back-calculated (in tunnelling) from some of the young geologies of Japan and Taiwan [12].

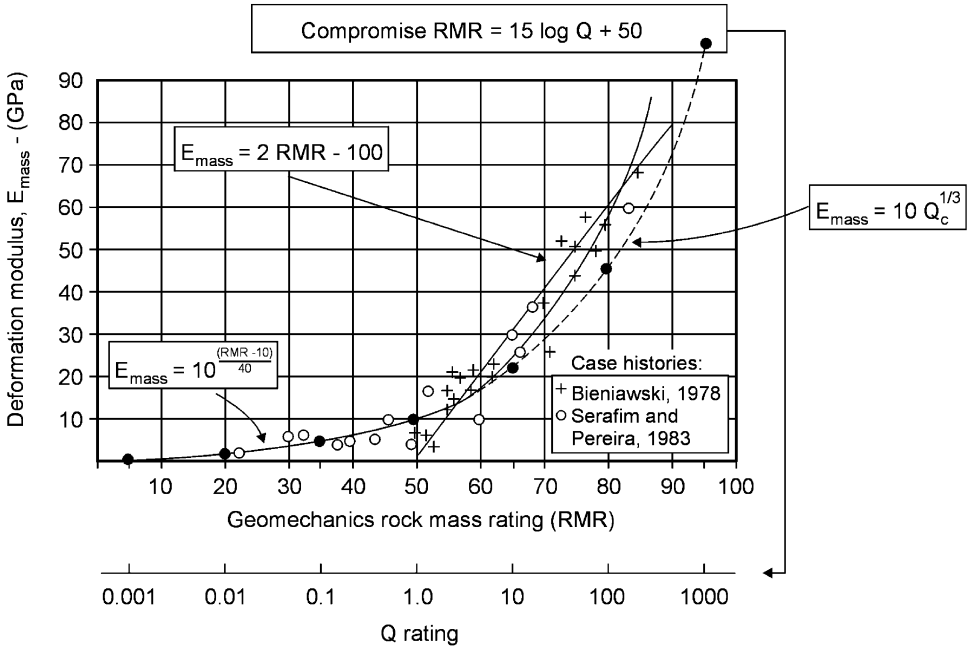

Fig. 7. Static deformation modulus E_{mass}, Q and RMR and some empirical inter-relationships [11,19–21].

6. Effects of stress and deformation on modulus and velocity

Thus far, the above discussion of deformation moduli has been devoid of depth or stress effects, at least beyond the typical plate load or tunnel relaxation magnitude. However there is evidence from deeper instrumented tunnels in competent rocks (where excavation disturbance is well controlled though never eliminated) that deformation moduli will also be subject to the positive effects of depth or stress effects, and the negative effects of porosity. There is evidence for this beyond the EDZ-affected, reduced modulus zone close to the opening, which also gives lower V_p.

The magnitude of depth-dependent moduli interpreted from three radial MPBX in a 1.6 km deep shaft in quartzites [24], varied from <2 GPa to more than 70 GPa, to take an extreme example. Perhaps we should traverse the $n > 1\%$ porosity lines in Fig. 4 to partly explain these EDZ and joint-porosity cases. Because of radial stress loss near the opening, we are already below the equivalent 'near-surface, low stress' line of nominal 25 m depth, and from there to the walls of the excavation, we have the increasingly negative effect of increased joint porosity, which may be largely unseen in relation to the logged rock mass quality.

Near-surface seismic refraction data for artificially stripped rock foundations, together with related Q-logging, do indeed suggest the need for sub-25 m depth, and $n > 1\%$ porosity lines of V_p versus Q_c for shallow foundations, following the trends shown in Fig. 4. Low foundation loads may also mobilise only the correspondingly lower ranges of deformation moduli. An SRF value of 2.5, appropriate to the characterisation of 'low stress, near-surface' conditions (from Table 13b, and related footnotes in the appendix) would be the most correct existing rating for Q-value estimation in such cases, though one may be tempted to use a higher SRF value (such as 5 or even 10) when within a very few metres of the surface, to more closely correlate with even lower moduli and velocities. (It should be noted that high values of SRF for loosening, and high values for adverse strength/stress ratios, are broadly speaking for similar purposes, namely to describe low-stress-driven, or high-stress-driven loosening.)

Over the past 50 years or so, numerous investigations of arch dam abutments have utilised simple seismic cross-hole (non-tomographic) measurements to extrapolate the static modulus of deformation results obtained from plate loading tests, to other parts of the foundation. Many such cases have recently been reviewed [12]. Such studies confirm the well-documented shortcomings of dynamic modulus estimates for civil engineering design in rock masses. When the compressional wave (V_p) and shear wave (V_s) velocities are used, with rock density γ, in the classic elastic (small strain) equation for calculating the *dynamic* Young's modulus (see compilations of equations in [12]):

$$E_{\text{dyn.}} = \gamma V_s^2 \frac{3(V_p/V_s)^2 - 4}{(V_p/V_s)^2 - 1} \tag{11}$$

significant over-estimates of the required modulus are obtained. The required *static* modulus of deformation is usually obtained from high-pressure plate loading (and similar) tests performed in carefully excavated test adits. The over-estimation of modulus is greatest for low quality rock masses at shallow depth, and least for excellent quality rock masses (e.g. $Q > 100$) measured at greater depths. Comparison of the three dynamic (Young's, shear and bulk) moduli is given in [9].

In order to bypass this site characterisation difficulty of $E_{\text{dyn}} > E_{\text{mass}}$, various empirical equations have been developed over the years, some of them for 'correction' of the dynamic moduli, others for estimating static moduli directly from rock mass quality measures such as RQD [1,12]. Such estimates can then be used together with the seismic P-wave velocities, for extrapolation of the drillcore-estimated moduli to 'inaccessible' parts of the rock mass. Although RQD, as a single parameter, is a quite sensitive measure of rock mass quality for rock engineering problems, it has undoubtedly been 'broadened' in scope by incorporation in RMR (as a rating) and in Q (directly). Since we have achieved an improved correlation between E_{mass} and Q_c, and between V_p and Q_c, it is logical to investigate a direct linkage between E_{mass} and V_p for use in civil engineering site investigations.

In Fig. 4, the assumption is made that seismic velocity V_p, and the static modulus of deformation are intimately inter-related. This supposition is first presented by elimination of Q_c (i.e. elimination of Q and σ_c) between Eqs. (4) and (9), then by making a further assumption of similar effects of porosity and depth on V_p and E_{mass}. The equation that is assumed to link V_p and E_{mass} is therefore:

$$E_{\text{mass}} = 10 \times 10^{(V_p - 3.5)/3} \tag{12}$$

The units of E_{mass} remain as GPa, and V_p as km/s. Table 1 shows this inter-relationship, and how each parameter may vary with the Q_c value, according to the source Eqs. (4) and (9).

There is seen to be an approximate doubling of the modulus and an increase of 1 km/s for each ten-fold increase of Q_c. Depths greater than the nominal 25 m for shallow refraction seismic, and porosities more than the nominal hard rock reference of 1% will have respectively, additive and subtractive effects on the above, following the graphic scheme shown in Fig. 4.

The combined effects of depth or stress that are believed to act on V_p *and* E_{mass}, can best be demonstrated by an example. The example is relevant to a generic nuclear waste repository of 500 m depth. It is

Table 1
Inter-relationships between V_p, E_{mass} and Q_c, based on Eqs. (4), (9) and (12)

Q_c	0.001	0.01	0.1	1.0	10	100	1000
V_p	0.5	1.5	2.5	3.5	4.5	5.5	6.5 km/s
E_{mass}	1.0	2.2	4.6	10	21.5	46.4	100 GPa

Note: nominal porosity = 1%, and nominal depth = 25 m.

designed to demonstrate the usual differences between conventional opinion (meaning one based on a near-surface or medium stress database) and depth or stress affected data. This is inevitably harder to find, since based on special projects such as the SKB Äspö ZEDEX project, or the UK Nirex Ltd Sellafield repository investigations, where in each case deep cross-hole seismic tomography was performed, and Q-values were known in detail from many kilometres of core logging [15,16,25].

Back-analysis of any deformations that have been measured gives the third leg of the data, which therefore includes Q-logging of core from the deep boreholes, deep cross-hole seismic tomography, and the MPBX extensometer data needed to back-calculate likely deformation moduli. In the case of the Äspö ZEDEX project [16], there were also the results of excavation logging of the Q-value. The mainly sub-millimetre size of measured deformations, imply very high 'stressed' moduli, which may be of the order of 60 GPa, based on simple continuum modelling.

For demonstration of potential depth effects, we will assume logged Q-values of 1, 5, and 20 and corresponding σ_c values of 100, 200 and 200 MPa. Following Eq. (3), this means Q_c values of 1, 10 and 40. Table 2 shows the estimated depth effect, and demonstrates the need to use data or predictions from depths relevant to the problem, in this case 500 m.

These stressed moduli and velocities are strictly for characterizing rock masses at depth. The increased moduli may be found to be representative of 'at depth' deformations, unless significant excavation disturbance is causing general loosening effects, like the increased joint porosity discussed earlier. It is also possible that different (i.e. high) SRF values are mobilised by adverse strength to stress ratios. Severe stress slabbing around excavations in massive highly stressed rock will be difficult to represent correctly in any numerical model. However, one may presume that in the radial (σ_r) direction, both the velocity (V_p) and the deformation modulus (E_{mass}) will be much reduced, especially in the outer few metres.

One may hope that this excavation effect in highly stressed massive rock is partly 'taken care of' by the high SRF values (shown in Table A6 (section b) in the appendix), but this of course is optimistic. The high SRF value would in any case need to be depth-or-radius limited, just as the need for yielding (end-anchored) rock bolts is limited to some few metres, usually in the range of $\frac{1}{2}$–1 radius in these hard rock cases.

In softer, less competent rock masses that may suffer squeezing even at moderate depth, a much thicker 'cylinder' of sheared and fractured ground may be involved. It is standard practice in countries like Japan, with Tertiary sediments prone to squeezing, to diverge motorway lanes in the approach to a tunnel with significant overburden, so that there are some five diameters of pillar between the two tunnels. This is to avoid unwanted interactions when driving the tunnels, of which there have been many.

Table 2
Contrasting predictions of near-surface, and deep or highly stressed velocities and moduli, based on Fig. 4

25 m depth Q_c	$V_p = 3.5 + \log Q_c$ V_p	500 m depth Q_c	$V_p = 5.0 + 0.5 \log Q_c$ V_p
(a) *P-wave velocity V_p (km/s)*			
1	3.5	1	5.0
10	4.5	10	5.5
40	5.0	40	5.8
25 m depth Q_c	$E_{mass} = 10Q_c^{1/3}$ E_{mass}	500 m depth Q_c	$E_{mass} = 10 \times 10^{(1.5+0.5 \log Q_c)/3}$ E_{mass}
(b) *Static deformation modulus E_{mass} (GPa)*			
1	10	1	12
10	22	10	46
40	34	40	58

There is direct evidence from the Pinglin Tunnel in Taiwan, of the potential for at least two diameters of sheared ground, judging from the partial closure of the 25 m distant pilot tunnel when advancing one of the main tunnels. In such cases there would be a corresponding tendency for a thicker 'cylinder' of modulus, strength and velocity reduction (and probably permeability increase). An elevated 'squeezing SRF' value would need to apply to this much larger volume. The length of appropriate rock bolts, preferably of the yielding variety like RFP (fibre-reinforced plastic) would also be increased to assist in the eventual stabilisation.

Fully grouted steel bolts of at least a tunnel diameter in length, in a 1000 m deep tunnel in Japan, 'registered' a thick cylinder of yielding ground, due to both squeezing and some swelling of the heavily stressed, hydrothermally altered granite. In retrospect, the bolts proved to be too stiff when fully grouted, and due to many tensile failures, there was a requirement for more than 1 km of bolts per running metre of tunnel [26]. This is also evidence of a thick disturbed zone, probably also having the changes of properties discussed above. In the non-NATM section of the same tunnel, a much stiffer double-bottom-heading Japanese method of tunnelling, using mass-concrete-embedded steel arches of almost 1 m in section, resulted in much smaller strains (but probably bigger support pressure) which most likely would have reduced the thickness of the EDZ, and perhaps altered some of the above property changes to *increases*, due to high tangential stresses closer to the opening [12].

Clearly we must also be aware that each of these potential property changes may tend to be anisotropically distributed. The modeller's description of a so-called 'plastic' zone may in reality be localised 'log spiral' shear surfaces or zones of block rotation, as observed respectively in physical models of continua for borehole stability [27], and in discontinua used for modelling tunnels and caverns [28].

When contemplating using 'stressed' moduli in numerical models such as UDEC-BB or 3DEC, where a tempting alternative for some modellers might be an FEM, FLAC or FLAC3D continuum model, one should be aware of the consequences of using the above, isotropic, stressed moduli. The distinct element models will develop their own, perhaps anisotropic EDZ, following the near-excavation response of the modelled jointing. In other words, if *numerical* plate loading tests or velocity measurements were carried out, the jointed models would certainly give evidence of reduced E_{mass} and V_p, perhaps with anisotropic distributions. This 'realism' cannot be registered correctly in continuum models, even when inserting a more deformable zone adjacent to the future excavations. There may then also be problems with artificial response in the case of anisotropic stresses. Artificial bulging may occur due to the lower moduli applied close to the excavations. The bulging is unlikely to be across the same diameter as in reality, if jointing is involved.

7. Effects of anisotropy on V_p, E_{mass} and rock mass strength

It is unfortunately easy to forget the consequences of anisotropic rock material and rock mass properties when contemplating the use of classification methods to derive ballpark input data for numerical models or for empirical design. In the laboratory sample, foliation and schistocity and sedimentation layering may each give anisotropic E-moduli, anisotropic V_p, and quite variable ratios of σ_c/I_{50}, or compressive to point load tensile strengths [12,29].

At rock mass scale, anisotropic horizontal principal stresses, probably combined with anisotropically distributed joint set frequencies and joint set properties, will tend to give anisotropic velocities, moduli and permeability, the latter especially marked sometimes, due to the sensitivity of joint apertures to stress, and the 'cubic' tendency of flow rate in relation to joint aperture. Ratios of principal permeability tensor magnitudes in the range 2–200, using multiple-hole hydrotomography methods, have been regularly recorded in Brazil [30].

When velocity profiles are measured at 15° or 30° intervals around the compass, elliptical distributions of velocity tend to be recorded [31,32]. This may be a combination of obviously dominant jointing trends, and in situ stress anisotropy, the two of which may be linked. Velocity anisotropy of 0.5 or even 1.0 km/s may be registered.

In other situations caused by cyclical bedding of say marl and sandstone, perpendicular and parallel measurement of deformation modulus beneath instrumented plate load tests [33], clearly show the anisotropy (in this case, orthotropy) of both E_{mass} and V_p, and their inter-relation. Fig. 8 shows a plot of E_{mass} versus $(V_p)^2$, with the near-surface results (A1, B1, C1 and D1) distributed along the lower $E_{mass}-(V_p)^2$ trend line, and the deeper results along a higher trend line. Although there are variations in the layer properties, there is a clear separation of the perpendicular (C and D) results from the parallel-to-layering (A and B) results.

When developing a rock mass strength estimate for comparison with TBM cutter forces of say 15, 25 or 30 t, an oriented Q-value, termed Q_0 was defined [29], which specifically used an RQD value oriented in the tunnelling direction. This was termed RQD_0. The subsequent oriented strength estimate for mostly compressive, as opposed to mostly tensile related failure, was estimated using Q_c together with rock density (γ) which is easily measured, and which gives

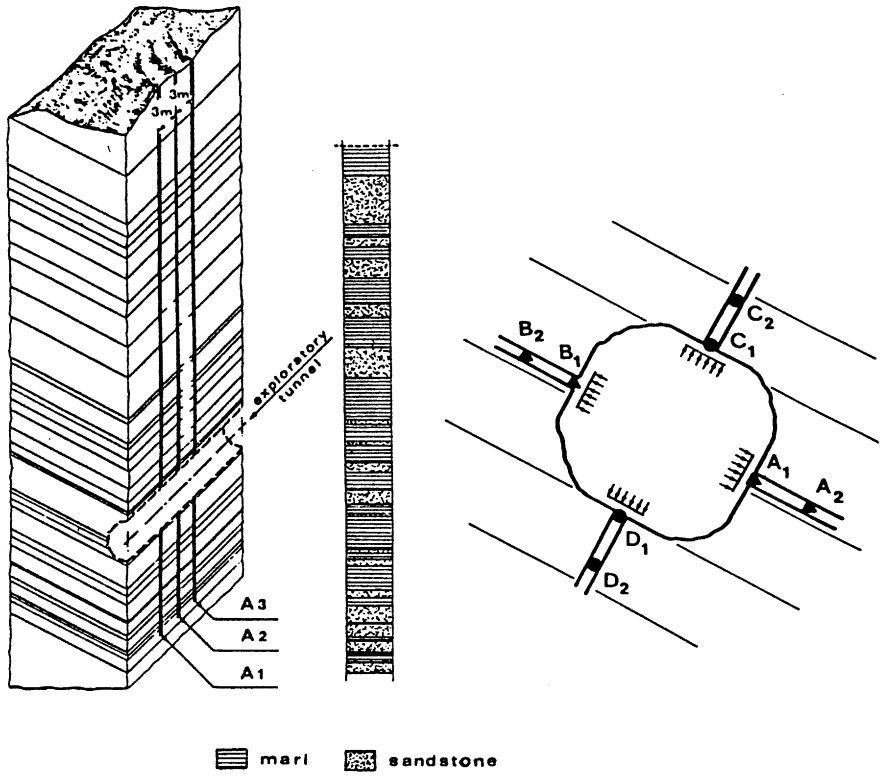

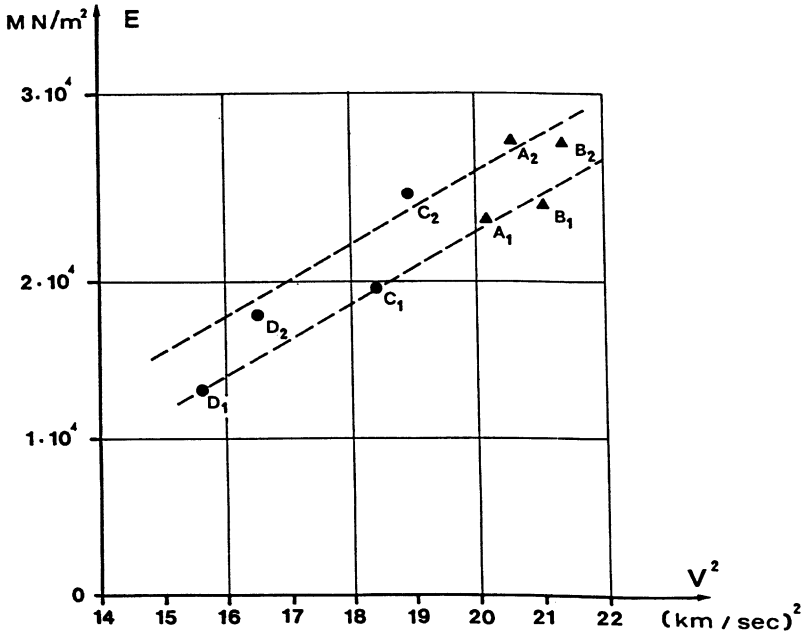

Fig. 8. Marl-sandstone inter-beds, giving anisotropic (or orthotropic) E_{mass} and V_p^2 results in a test gallery [33]. The shallowest measurements show lowest E_{mass} results as a group, compared to the deepest measurements (the EDZ result), while the perpendicular to bedding measurements are generally lower than the parallel to bedding ones (the orthotropic result).

some additional sensitivity to reduced or increased porosity, following a modification of [34] to give better sensitivity to rock type

$$\mathrm{SIGMA}_{cm} = 5\gamma Q_c^{1/3} \quad (13)$$

where $Q_c = Q_0 \times \sigma_c/100$ as from Eq. (3), but with RQD_0 in place of RQD in the Q calculation. J_r and J_a were for the joint set or discontinuity that most affected the rock mass failure under the cutter. γ is the rock density in t/m^3.

In the case of markedly schistose or foliated rock, which tend to have low point load (I_{50}) strengths, ratios of σ_c/I_{50} may be far higher than the typical ratio of about 25, so an 'accommodation' was made for the likelihood of combined tensile and shear related failure, across and along the planes of reduced strength [29]. In this case another relation was used, but using the same normalisation principle:

$$\mathrm{SIGMA}_{tm} = 5\gamma Q_t^{1/3} \tag{14}$$

where $Q_t = Q_0 \times I_{50}/4$, to distinguish the strongly anisotropic rock materials that have ratios of σ_c/I_{50} far greater than the typical value of about 25, commonly found with more isotropic rocks. The above normalisations therefore give $\mathrm{SIGMA}_{cm} > \mathrm{SIGMA}_{tm}$ when the matrix is anisotropic.

Using these two devices to account for anisotropic strength and structure, Q_c and Q_t are capable of capturing at least some of the anisotropy known to affect rock material and rock masses. It remains to be seen the extent to which the newly defined Q_c and Q_t terms give an improved estimate of E_{mass} and V_p, using the equations already presented here. However, it is obviously logical to use RQD_0 and the most relevant J_r and J_a values when attempting to derive estimates of moduli and velocities, both of which are quite likely to be direction dependent. The loading or measurement direction should therefore be considered. In principle and where possible, Q_0 which contains an oriented RQD_0, should replace Q, when estimating Q_c for use in the earlier correlation equations. Readers can refer to the list of nomenclature for clarifying these Q, Q_c, Q_t and Q_0 terms, where however, there will be found more uses for the symbol Q, if geophysics is included in the discussion.

8. Support pressure

The original Q-based empirical equation for underground excavation support pressure [3], when converted from the original units of kg/cm^2 to MPa, is expressed as follows:

$$P_r = \frac{J_r}{(20 \times Q^{1/3})} \tag{15}$$

This means that when, for simplicity, we set J_r to a typical value of 2 (for the case of 'smooth, undulating' joints, see Table A3 (section a) in the appendix) we obtain a very simple inter-relation between P_r and E_{mass}. Firstly, we have:

$$P_r = 0.1Q^{-1/3} \tag{16}$$

Therefore it follows from Eq. (9), with $\sigma_c = 100$ MPa, that

$$P_r \approx \frac{1}{E_{mass}} \tag{17}$$

where P_r is in MPa and E_{mass} is in GPa.

This surprising though not illogical inverse proportionality is shown in Table 3, to demonstrate that support pressure magnitudes vary strongly with Q-value. Note that rock bolts of 20 t capacity, installed at 2.0×2.0 m centres, provide a theoretical 5 t/m^2 capacity, and correspond to the needs of a $Q = 8$ rock mass. This is if we ignore the beneficial effects of fibre reinforced shotcrete S(fr), which actually has a very positive effect in reduced bolting needs, which one can readily observe by inspecting the support recommendations given in Fig. 1. Bolts can be more widely spaced due to the cohesive (surface-binding) and structural-supporting effect of S(fr), the latter only if the shotcrete is applied thickly enough.

Inspection of the Q-system support pressure diagram [3] indicates, as does Table 3, that there is an expectation of an approximate doubling of the support capacity needs, as the Q-value reduces by successive orders of magnitude. As we have also seen, the deformation modulus appears to be roughly halved for each ten-fold reduction in Q-value due to the approximate inversion shown above.

There is increasing evidence that the support pressure 'rules' in the Q-system do indeed follow these strongly Q-value dependent trends. A comprehensively instrumented hydropower cavern in multiply faulted sedimentary rock demonstrated the need of almost 0.4 MPa support pressure in the form of bolts and instrumented high capacity cables [35]. The deliberately inclined, (non-radial) Q-system-based wall support was heavily loaded by joint and discontinuity shear while reaching equilibrium, but later survived a devastating, magnitude 7.3 earthquake with an uncomfortably close epicentre.

9. Possible correlations between the Q-value, $Q_{seismic}$ and the Lugeon value, due to jointing

A wide ranging review of seismic measurements in rock engineering and the geological sciences [12] has unearthed interesting data from different disciplines, suggesting some useful, cross-discipline relationships. One is the *approximate* similarity between the rock mass quality Q-value used in rock engineering, and the so-called seismic quality factor used in geophysics, which here we must term Q_{seis} (where Q_{seis} is the inverse of attenuation). Q_{seis} is usually defined as the maximum energy stored in a cycle divided by the energy lost during the cycle. It is of course quite logical that massive, high

Table 3
Some simplified inter-relationships between Q, P_r and E_{mass}. In these examples, J_r is assumed = 2 and $\sigma_c = 100$ MPa, to demonstrate the potential inverse symmetry

Q	0.001	0.01	0.1	1.0	10	100	1000	
E_{mass}	1.0	2.2	4.6	10	21.5	46.4	100	GPa
P_r	1.0	0.46	0.22	0.1	0.05	0.02	0.01	MPa
P_r	100	46.4	21.5	10	4.65	2.15	1.0	t/m^2

Q-value rock masses cause limited attenuation of seismic waves (hence they also tend to have high values of Q_{seis}), whereas heavily jointed, clay-bearing rock masses with low Q-values cause strong attenuation of seismic waves, and have low values of seismic quality (Q_{seis}) as a result.

Geophysicists consider Q_{seis} (actually its P- and S-wave components termed 'Q_p' and 'Q_s') to be fundamental rock properties, despite the complication of frequency-dependence in the case of fluid-bearing porous rock or rock masses. There is also a geophysical 'Q_c' term for the seismic quality of the coda, which is the 'tail end' of the recorded dynamic waves, after they have passed through large volumes of rock mass in the upper crust, following energy release from nearby earthquakes. See review of many examples in [12]. The coda gives an average 'quality', which is the end result of attenuation due to fluid movements, and due to intrinsic scattering of the seismic waves, after passing through large volumes of jointed and faulted rock (and lithologic boundaries) that are likely to be under the influence of effective stresses of many tens or hundreds of MPa.

Pore fluid and joint fluid movement during the passage of seismic waves, so-called 'squirt', is believed to be responsible for much of the attenuation (and lower values of Q_{seis}) at lower frequencies, while pore space and joint and fault structures that cause intrinsic scattering of the seismic waves represent the components most responsible for attenuation at high frequencies. As a rough rule-of-thumb, the P-wave component of what we have termed Q_{seis} (to avoid confusing our rock engineering Q_c term with geophysicist's 'Q_c') generally ranges from extremes of about 5–5000. Frequency, depth and rock quality each play a role in determining this range, with massive rock at great depth giving the highest values, due to least attenuation. In contrast, the rock engineer's rock mass quality Q_c may range from extremes of 10^{-5}–10^4, when using a full range of uniaxial compression strengths of roughly 1–400 MPa [12].

Another interesting 'inter-discipline' result concerns the independent measurement of the P-wave velocity and the Lugeon value at two French dam sites in crystalline rocks [36]. These, and other related data, imply a potential linkage between Lugeon value and Q-value, at least where permeability is caused by different degrees of joint connectivity.

The graph of V_p versus Lugeon value shown in Fig. 9 suggests an upper-bound relationship between V_p and L. As shown in the inset of Fig. 9, if we utilise Eq. (4) relating V_p and Q_c, we can place a tentative Q_c scale along the lower axis of this set of results.

The dotted line that has been added to the data (and exactly parallels some of the trends) has the remarkably simple relation:

$$L \approx \frac{1}{Q_c}. \tag{18}$$

This is due to the symmetry of the two V_p relationships given in the figure, giving $\log Q_c = (-)\log L$. The Q_c scale added along the lower axis is strictly only applicable to nominal, near-surface (25 m depth) seismic data, following Eq. (4) which describes the central trend in Fig. 4. The Q_c scale would therefore need to be shifted to the right as depth increased, to match reductions of Lugeon values, which of course also occur as a result of higher Q_c values.

For a given Lugeon value, the higher or lower velocities imply that depth of measurement was deeper or shallower, respectively. The mechanism needed to explain reduced Lugeon values in the region $V_p = 2.5-3.5$ km/s, might perhaps be reduced injection pressures in nearer-the-surface rock, preventing joint deformation effects.

Since discovering this potential trend, many data sets have been explored [12]. By chance, or perhaps because of the suggested trend, thousands of water well data from Swedish and Finnish nuclear-waste related studies, consistently show medium depth permeability ranges from about 10^{-4}–10^{-10} m/s. Since 1 Lugeon is approximately equal to 10^{-7} m/s (1.3×10^{-7} based on a porous medium interpretation) we may risk an interpretation that the Swedish and Finnish bedrock may be indicating a range of rock qualities across the whole range of Q-values from 0.001 to 1000. Perhaps significant of coupled behaviour [7], at depths in the 500–1000 m range, there is a trend for values down to about 10^{-11} m/s. It would be of great interest to know the range of seismic velocities operating over the range of permeabilities and depths cited above. *Perhaps* the range is as wide as 0.5–6.5 km/s. The lower range may however be truncated by depth or stress effects.

Of course there will be problems with this 'simple' model, where clay is causing a disproportionate reduction in the Q-value (as expected) and a reduction in permeability (contrary to this simple model). Perhaps in

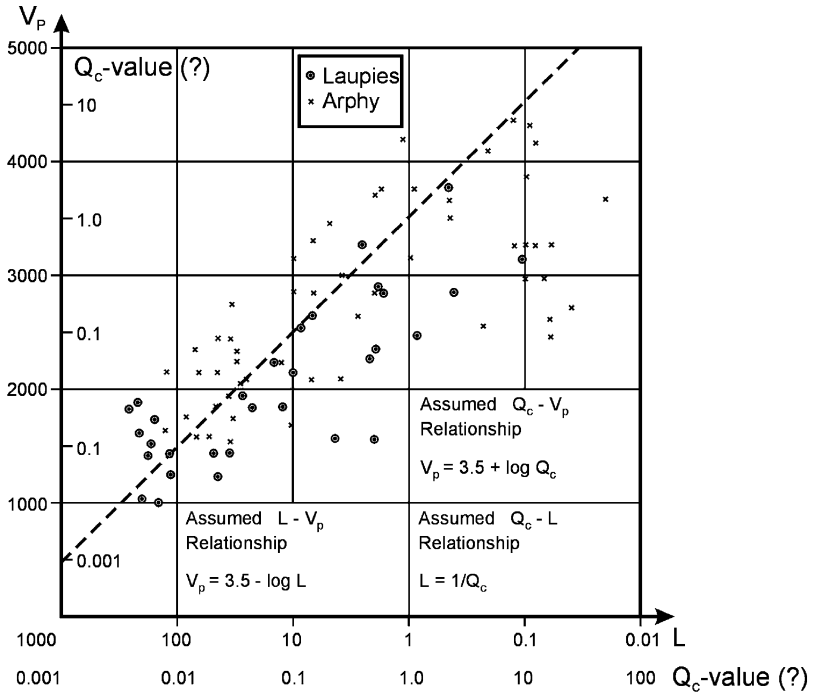

Fig. 9. Dam site comparison of Lugeon values with P-wave velocities [36]. Tentative $Q_c - L$ correlation from [2] which will strictly correlate only to the nominal, near-surface (25 m depth) sets of measurements. Low Lugeon values with low velocities may correspond to reduced injection pressures, therefore reducing joint deformation effects.

broad areas of variably jointed rock, with $Q = 0.1-100$, the model holds some truth. In general terms, low Q-values suggest greater connectivity and high Q-values suggest the opposite trend, giving credence to a link with high pressure (i.e. deforming, Lugeon-based) injection test results.

In a simplified theoretical exploration of the problem [12] it has been shown that if most flow is channelled in one joint set, and further, if the highest flow rate is actually occurring in one of these joints (one with greatest aperture that preferentially takes flow from others due to coupled behaviour) then some simple theoretical models can be used to explain the reasonableness of Eq. (18).

Firstly, the radial flow equation can be utilised for flow to or from a borehole crossing the joint and joint set in question. With near-perpendicular intersection there is a theoretical logarithmic decay in pressure away from an injecting borehole, if flow remains laminar. Secondly, the deformation of *each side* of the joint taking most water, caused by up to 1 MPa reduction of effective stress, can be modelled with the Boussinesq equation. Due to the assumed cubic flow law ($k = e^2/12$, and flow rate proportional to e^3), and due also to the cube root proportionality of deformation modulus E_{mass} and Q_c (Eq. (9)), a typical result that may be obtained with a reasonable set of geometric assumptions, is that L is approximately equal to $1/Q_c$, as in Eq. (18).

Fig. 10 gives a tentative, but potentially integrated picture (a nomogram) of the inter-related or partially inter-related parameters Q_c, E_{mass}, V_p and L, and examples of where 'massive rock', 'jointed rock', etc. might plot as a function of depth. The left-hand vertical scale of Lugeon and V_p is derived from the trend shown in Fig. 9, i.e. $V_p = 3.5 - \log L$. It is not at present known the extent to which the depth lines in Fig. 10 would fit this trend. However, it is perhaps reasonable to assume that increased depth and velocity, and reduced Lugeon values are inter-related. The Lugeon—Q_c scale along the bottom of the diagram is relevant only to the nominal, near-surface (25 m depth) Eq. (4) relationship, i.e. it applies to the central (solid) diagonal in the figure. The Q_c scale, from Fig. 4 should be considered 'fixed', while the Lugeon scale would be expected to shift to the left for predictions at greater depth than the nominal 25 m. Unfortunately, the porosity correction for E_{mass} and V_p cannot be applied to the Lugeon approximation, as increased porosity will usually lead to higher permeability. Despite this known shortcoming, the figure is presented here as a stimulus to further research and subsequent improvement.

10. Tunnel or cavern deformation

After several years of collecting tunnel deformation (i.e. convergence) and Q-value data—which was actually the original purpose of developing a rock mass classification system [3], a collection of Q/SPAN versus deformation data was published, having both axes as log

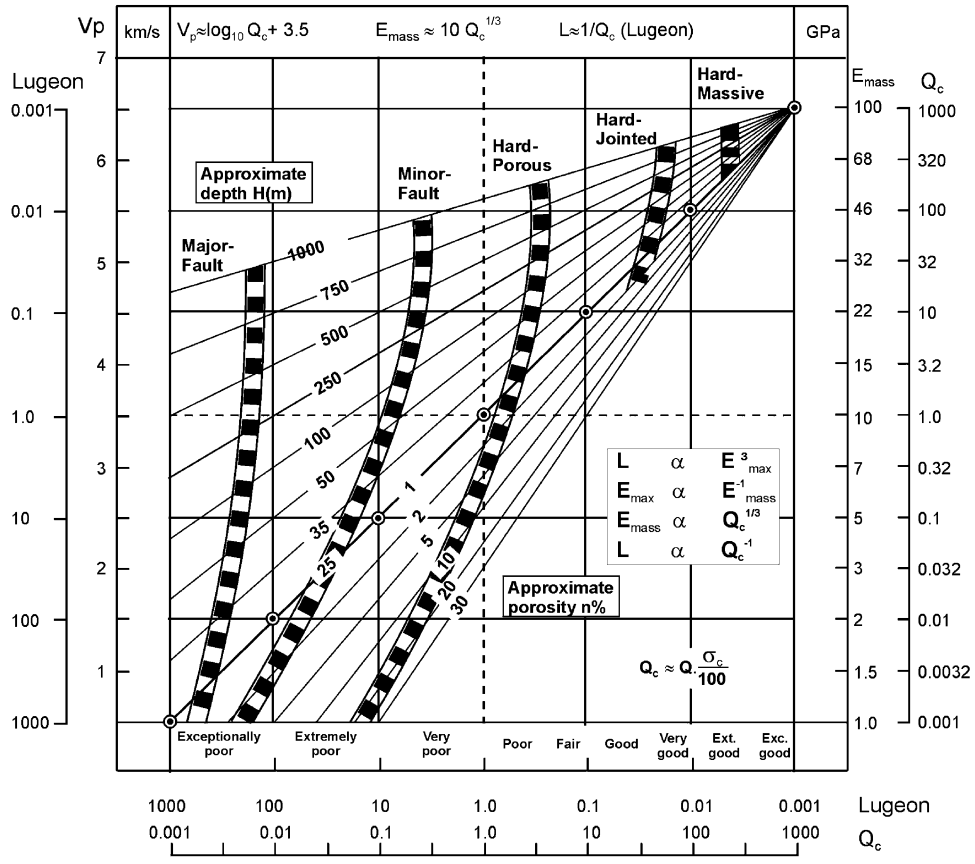

Fig. 10. Elements of potential geohydrologic integration, using $Q_c - V_p - E_{mass} - L$ and depth, to indicate potential type curves for rock masses [2]. Depth effects on Lugeon results are tentative, and the porosity correction obviously applies only to velocity and modulus.

scales [17]. Approximately linear trends of data were seen with this form of plot. Subsequently, data from the several stages of excavation of the 62 m span Gjøvik Olympic cavern were added, using the pre-installed MPBX monitoring data. There were temporary spans of 10 and 35 m for the pilot tunnel and large top heading. At each stage, Q-logging was performed. The updated plot from [6] is reproduced in Fig. 11a.

By good fortune, Chen and Guo collected hundreds of fresh data from difficult tunnelling projects in Taiwan, using the same plotting format of log Q/SPAN and log *convergence*. They kindly made this Chinese language article available [37]. One of their figures is reproduced in Fig. 11b. Some time later, noticing the continued downward trend of this convergence data, the equation of the central line, representing roughly half the convergence was derived almost by inspection. It proved to have the following 'familiar' simplicity:

$$\Delta = \frac{\text{SPAN}}{Q} \tag{19}$$

(where SPAN is expressed in metres, and Δ is in millimetres).

As has been pointed out elsewhere, the spread of data is rather large, and the above trend is a curiosity, until explained. Attempts were therefore made to 'explain' the ranges of data, using something resembling the competence factor (i.e. the strength/stress ratio) as used to evaluate SRF in the case of classification of likely conditions when excavating in massive rock masses. (Table A6 (section b), appendix). The forms of equation shown below were finally chosen:

$$\Delta_v = \frac{\text{SPAN}}{100Q}\sqrt{\frac{\sigma_v}{\sigma_c}} \tag{20}$$

$$\Delta_h = \frac{\text{HEIGHT}}{100Q}\sqrt{\frac{\sigma_h}{\sigma_c}} \tag{21}$$

Therefore we can also give an approximation for $k_0 = \sigma_h/\sigma_v$ as follows:

$$k_0 = \left(\frac{\text{SPAN}}{\text{HEIGHT}}\right)^2 \left(\frac{\Delta_h}{\Delta_v}\right)^2 \tag{22}$$

Units in Eqs. (20)–(22) are as follows: SPAN, HEIGHT, Δ_v and Δ_h are each in millimetres, while rock stresses and rock strengths need consistent units such as MPa.

It should be carefully noted that if very low Q-values are used in these equations (i.e. Q-values that exist prior to pre-treatment) then very large (perhaps metre-size) deformations will be predicted by Eqs. (20)–(22). This

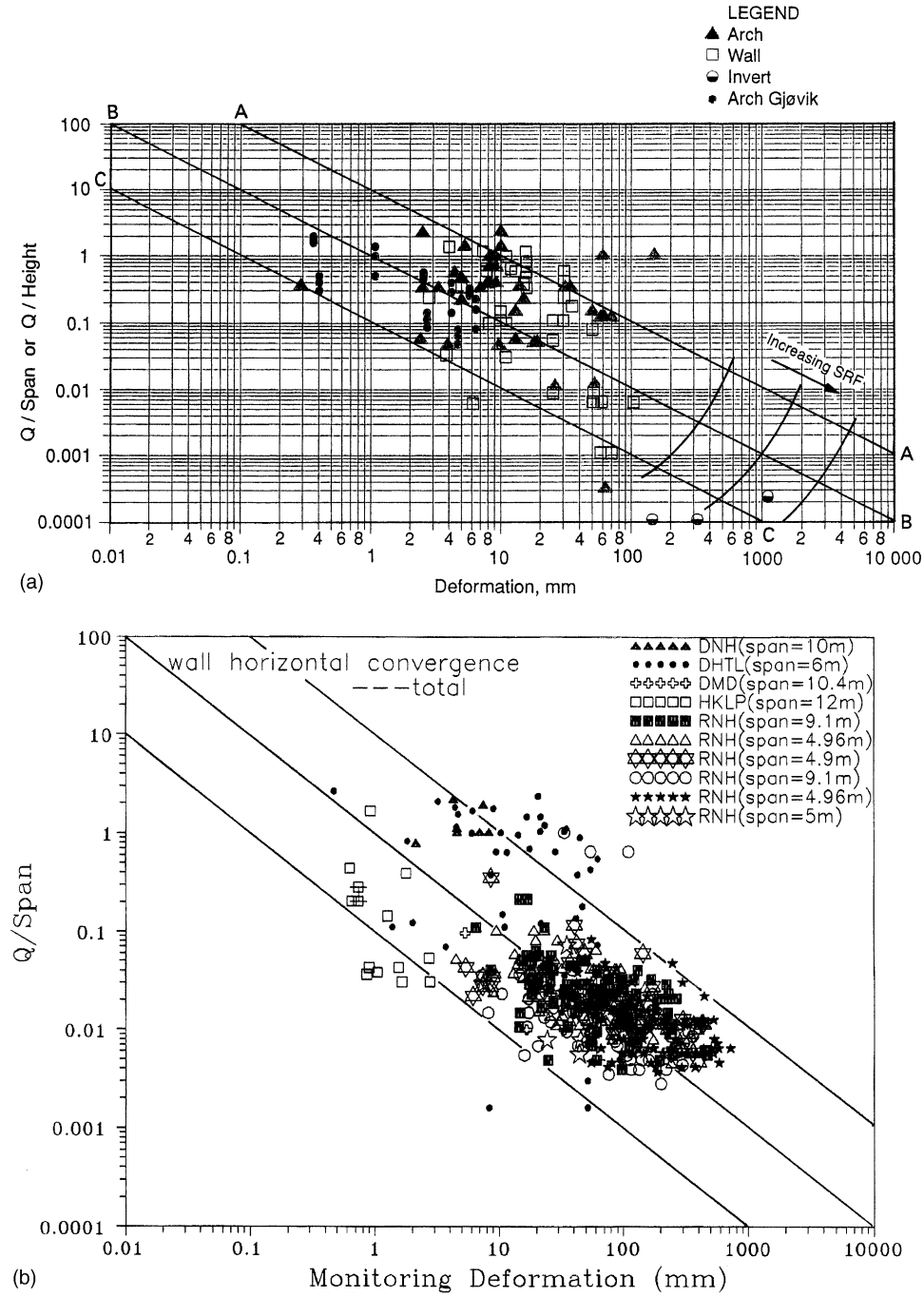

Fig. 11. (a) SPAN/Q versus radial deformation and convergence data for tunnels and caverns, from [6]. (b) Extensive new convergence data from Taiwan [37].

appears to be a shortcoming, but perhaps it is correct. If the planned tunnels were opened without rock mass improvement, i.e. drainage, pre-grouting, spiling, etc. then metre-size deformations or collapses would certainly be expected. Let us cite the Pinglin Tunnel again, where heavily jointed, slickensided and sometimes clay-bearing quartzites are acted on by exceptionally high joint-water pressures. An initial Q-value, prior to eventual drainage, of about:

$$Q = \frac{15}{9} \times \frac{0.5}{4} \times \frac{0.05}{1} = 0.01$$

will imply a potential deformation of about 1 m, using the simple relation of Eq. (19). The reality is actually repeatedly stuck TBM, and sometimes badly deformed steel sets, or occasional piping failures at the face as the

water tries to drain through probe holes. In a recent tragic occurrence, one of the tunnels, by now with a drill-and-blasted top-heading, was rapidly filled with about 7000 m^3 of quartz debris, where conditions were probably even worse than the above. The tunnel 'face' was suddenly retreated by 100 m. A key to 'improved' Q-value and reduced deformations, would be drainage if achievable, and effective high pressure pre-grouting. These two potential measures can be beneficial to one or to several of the six Q-parameters, respectively, as will be demonstrated later.

We can take another real example, this time not extreme—a hydropower cavern of 20 m span and 50 m height [38]. Vertical and horizontal stresses were reportedly about 6 and 4 MPa respectively. The uniaxial strength was about 35 MPa, and the Q-value about 3. Measured deformations, where MPBX were installed, were approximately 25 mm in the arch and often about 50–55 mm in the walls, but with significant variation here. Eqs. (20) and (21) predict deformations of 28 and 56 mm respectively, while Eq. (22) predicts:

$$k_0 = \left(\frac{20}{50}\right)^2 \times \left(\frac{56}{28}\right)^2 = 0.64$$

(which is close to the measured ratio of $4/6 = 0.66$).

It is important to note that the original trend of the data shown in Figs. 11a and b, namely inverse proportionality of deformation and Q-value is retained in the above equations. The 'fine-tuning' is designed to try to explain variable performance, though some of this will undoubtedly be due to over-conservative support (perhaps due to earlier tunnel stability problems). Such data would plot to the left in Figs. 11(a) and (b). Excavations with insufficient temporary support and consequently exaggerated problems later, might explain some of the data plotting to the right-hand side of the central trend line.

11. Exploring a deeper meaning behind the six components of Q

In earlier sections of this paper, we have explored some fundamental, though empirical Q-value correlations with two rock mass parameters useful for site investigation (V_p, L), four that may be useful for design (E_{mass}, $SIGMA_{cm}$, $SIGMA_{tm}$, and the expected support pressure P_r), and two that may be useful for predicting or interpreting underground excavation behaviour (Δ_v and Δ_h). Some of these empirical equations and interrelationships have been as simple as *inverse proportionalities* with the Q or Q_c value, suggesting perhaps, that in the case of Q or Q_c, we could be dealing with a fundamental rock mass parameter, or a combination of rock mass parameters. Soon we will see that Q_c (and even Q) can reasonably be claimed to have units of MPa, or very nearly so.

When developing the Q-system in 1973, first two parameters (RQD/J_n), then four ($RQD/J_n \times J_r/J_a$), penultimately five (with SRF) and finally six parameters (with J_w) were created to constitute the final Q-value [3]. Their individual ratings were derived (and successively fine-tuned) by trial-and-error, during back-analysis of 212 case records. The magnitude of Q as a scale of quality, was matched with different thicknesses of shotcrete (plain or mesh-reinforced, or none at all) which mostly took care of the 'cohesive' weakness or strength of individual rock masses. Block size and number of joint sets was particularly important here. Q was also matched with different spacings and capacities of rock bolts and cable anchors. Sometimes none were found necessary by those who designed and constructed the tunnels and caverns used in the back-analyses.

The original instructions for choosing appropriate amounts of shotcrete and/or rock bolts were based on the 'conditional factors' RQD/J_n and J_r/J_a, which distinguished between the greater need for shotcrete ('cohesive support') when block sizes were small (low RQD/J_n) and conversely, the greater need for rock bolts when frictional strength was low (low J_r/J_a) *and* block size was large (higher RQD/J_n) [3].

The need for bolting can be assumed in principle to be tied to a need for increased frictional strength within the rock mass, to avoid immediate block-falls and future over-break, to avoid deep wedge failures (in the arch or walls) and to protect the shotcrete from shear failure or bond failure. The timely application of bolting helps to retain peak shear strength and dilatant joint behaviour if there is roughness. The larger deformations that may already occur at the face in the case of clay-bearing joints and filled discontinuities may imply post-peak shear resistance, and even contractile behaviour, unless heavily over-consolidated clay fillings are still in operation (prior to their potential strain-softening and water uptake).

11.1. The frictional component

The dual reinforcement of the 'cohesive component' and 'frictional component' concept can be taken further by referring to the fact that the ratio J_r/J_a closely resembles the dilatant or contractile coefficient of friction for joints and filled discontinuities. This was discovered *after* the six Q-parameters and their ratings were finalised, and is demonstrated in Fig. 12, where the three forms of 'rock-to-rock' contact are also illustrated, using illustrative shear strength-displacement graphs. Relative magnitudes of $\tan^{-1}$ (J_r/J_a) imply that the back-calculation of case records and fine-tuning of ratings, has given surprisingly realistic $\phi + i$, or ϕ, or

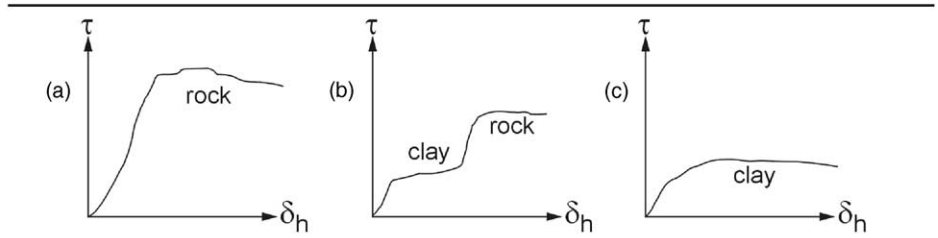

(a) Rock wall contact	J_a/J_r =	(thin coatings) 0.75	1.0	2	3	4
		$\tan^{-1}(Jr/Ja)°$				
A. Discontinuous joints	4	79°	76°	63°	53°	45°
B. Rough, undulating	3	76°	72°	56°	45°	37°
C. Smooth, undulating	2	69°	63°	45°	34°	27°
D. Slickensided, undulating	1.5	63°	56°	37°	27°	21°
E. Rough, planar	1.5	63°	56°	37°	27°	21°
F. Smooth, planar	1.0	53°	45°	27°	18°	14°
G. Slickensided, planar	0.5	34°	27°	14°	9.5°	7.1°

(b) Rock wall contact when sheared	J_a/J_r =	(thin fillings) 4	6	8	12
		$\tan^{-1}(Jr/Ja)°$			
A. Discontinuous joints	4	45°	34°	27°	18°
B. Rough, undulating	3	37°	27°	21°	14°
C. Smooth, undulating	2	27°	18°	14°	9.5°
D. Slickensided, undulating	1.5	21°	14°	11°	7.1°
E. Rough, planar	1.5	21°	14°	11°	7.1°
F. Smooth, planar	1.0	14°	9.5°	7.1°	4.7°
G. Slickensided, planar	0.5	7°	4.7°	3.6°	2.4°

(c) No rock wall contact when sheared	J_a/J_r =	(thick fillings) 5	6	8	12	13	16	20
		$\tan^{-1}(Jr/Ja)°$						
Nominal roughness of discontinuity rock walls	1.0	11.3°	9.5°	7.1°	4.8°	4.4°	3.6°	2.9°

Fig. 12. (a–c) Inter-block frictional behaviour—an extract from the J_r and J_a rating tables from the appendix. $\mathrm{Tan}^{-1}(J_r/J_a)$ shows apparently dilatant ($\phi + i$) friction angles for many joints, and apparently contractile ($\phi - i$) friction angles for many mineral filled discontinuities.

$\phi - i$ estimates of the operating 'friction angles', from the extremes of clean-and-rough-and-discontinuous (79°) to slickensided-and-thinly clay-filled (2°). Category (c)—'no rock-to-rock contact' uses a nominal $J_r = 1.0$ and J_a values ranging up to an extreme of 20. The value of $\tan^{-1}$ (1/20) is in this case close to 3°. (See Tables A3 and A4 in the appendix.)

As geotechnically trained engineers, we can visualise that the necessary addition of J_w as the last and 6th parameter of Q, was for 'fine tuning' this J_r/J_a ratio, adding something like a softening and an effective stress correction for when water was present. The parameter J_w was also designed to roughly account for stability problems due to combinations of high water pressures, high permeabilities, and potentially high storativity (see J_w descriptions in Table A5 in the appendix).

As observed earlier, J_w may sometimes need to take care of the risk of piping, during which the shear resistance of the rock mass nearly disappears, as witness the filling of 100 m of a tunnel, initially through a probe hole in the face, with hard, 200–300 MPa jointed quartz debris, of centimetre to metre size, together with water and some clay [39]. This would have been an event of $J_w = 0.05$ magnitude, as needed recently in some other extreme conditions of 'debris' release (blocks, sands, gravels) and water flooding in Italy and Kashmir. Unfortunately both these were TBM–driven tunnels. Inevitably, some of the TBM involved were eventually abandoned in favour of drill-and-blast (and related techniques), after years of struggles with the machines in 'impossible' conditions.

With the above in mind, the 'frictional component' (FC) of a rock mass will be defined as follows, and examples of typical magnitudes will be given shortly:

$$\mathrm{FC} = \tan^{-1}\left(\frac{J_r}{J_a} \times J_w\right) \quad (23)$$

It is logical to assume that by using J_r/J_a ratings relevant to the joints or discontinuities most affecting the result of the particular loading direction, one will tend to get a result that is sensitive to anisotropic joint properties. As defined, J_r and J_a will tend to give the minimum frictional component FC.

11.2. The cohesive component

Addressing our attention to the remaining Q-parameters, we may observe that RQD/J_n represents relative block size. This ratio was used in [5], to identify rockburst-prone hard rock masses, which, because of sparse jointing, will tend to have RQD/J_n ratios in the range 25–200, as opposed to typical jointed rock RQD/J_n ratios from 10, to as little as 0.5. Massive, highly stressed rock masses with high cohesive strength suffer the greatest reduction in block-size and cohesive strength, as a result of stress-induced fracturing around deep excavations. However, this does not occur prior to excavation, so the *characterisation* rating and the empirical tunnel design *classification* rating may differ considerably. (See footnotes beneath the SRF ratings, Table A6 (section b) in the appendix.)

As in the frictional cases that needed 'fine tuning' and adjusting for effective stress with J_w, we may speculate that SRF was a necessary 'fine tuning' and adjustment for the effects of stress (and sometimes fragmentation) in the case of relative block size and 'cohesive strength'. We needed to account for the adverse effect of excavating an opening in an over-stressed (or sometimes under-stressed) rock mass. In the case of competent rock, SRF is a measure of the stress/strength ratio, in anticipation of a stress-fractured EDZ in previously quite massive rock, requiring heavy, but yielding support. When SRF applies to faulting, the idea of loosening due to previously fractured (i.e. faulted material) is also relevant. The less frequently used SRF categories of squeezing and swelling are also indicative of a shear-displacement-reduced or swelling-strain-reduced 'cohesive strength' (or rather, weakness), together with the presence of an unbalanced driving force or increased radial stress σ_r, in each case requiring heavier support to resist the effects of the *tangentially* strained EDZ.

A cohesive component (CC) consisting of the three remaining Q-parameters, applied in the correct numerical format, can be generalised and improved by normalisation with $\sigma_c/100$, as in the case of Q_c. The cohesive component CC is therefore expressed as follows:

$$\mathrm{CC} = \frac{\mathrm{RQD}}{J_n} \times \frac{1}{\mathrm{SRF}} \times \frac{\sigma_c}{100} \quad (24)$$

In highly anisotropic rock, having high ratios of σ_c/I_{50}, it is logical to assume that by replacing $\sigma_c/100$ with $I_{50}/4$ (as in Eq. (14)) one will produce a more 'accurate' result. The potential anisotropy of CC could be further improved by selecting RQD_0, i.e. RQD in the loading direction.

11.3. Examples of FC and CC

We are now in a position to tabulate examples, starting with FC, to illustrate the surprising realism of the two components of Q_c (See Tables 4 and 5).

It may be reasonable to speculate that when many case records were closely grouped in the original SPAN/ESR versus Q graphs [3], there would tend to have been more 'reliability' in the original Q-parameter ratings, and therefore perhaps in the realism of the above FC and CC components. In very massive rock requiring no support, the partial safety factors governing, for example, mobilised friction and mobilised cohesion, will be unknown. Also in very poor rock that needed cast concrete linings, the load and strength levels would both tend to be uncertain. On the other hand in central areas of rock quality, such as $Q = 0.1-10$, the application of B + S or B + S(mr) was based on a host of case records, and on the possible observation of the need for more, or sometimes less support. Cracking of the shotcrete could have been observed, and stabilisation of the

Table 4
Five typical examples of FC (frictional component) estimation using Eq. (23). Refer to Tables A3–A5 in the appendix for the interpretation of the selected ratings

J_r	J_a	J_w	FC (deg)
2	1	1	63
1	1	1	45
1.5	2	0.66	26
1	4	0.66	9
1	6	0.5	5

Table 5
Five examples of CC (cohesive component) estimation using Eq. (24). Refer to Tables A1, A2 and A6 in the appendix for interpretation of the selected ratings

RQD	J_n	SRF	σ_c (MPa)	CC (MPa)
100	2	1	100	50
90	9	1	100	10
60	12	1	50	2.5
30	15	2.5	33	0.26
10	20	5	10	0.01

Table 6
Five progressively worsening rock mass qualities (from Tables 4 and 5), and their predicted near-surface properties. Consult all tables in the appendix for explanation of the selected ratings

RQD	J_n	J_r	J_a	J_w	SRF	Q	σ_c	Q_c	FC (deg)	CC MPa	V_p km/s	E_{mass} GPa	L
100	2	2	1	1	1	100	100	100	63	50	5.5	46	0.01
90	9	1	1	1	1	10	100	10	45	10	4.5	22	0.1
60	12	1.5	2	0.66	1	2.5	50	1.2	26	2.5	3.6	10.7	0.8
30	15	1	4	0.66	2.5	0.13	33	0.04	9	0.26	2.1	3.5	22.9
10	20	1	6	0.5	5	0.008	10	0.0008	5	0.01	0.4	0.9	1250

Note: FC applies only to the least favourable joint set or filled discontinuity, and should therefore not be used in isotropic models without due caution. The units of σ_c are MPa. A significant degree of anisotropy can be provided if desirable or relevant, by using oriented RQD_0 and values of J_r and J_a relevant to the loading or testing direction. The ratio $I_{50}/4$ can replace $\sigma_c/100$ in Eq. (24), if a further adjustment for matrix anisotropy is required. The effects of anisotropic stresses, and/or matrix porosity, on V_p and E_{mass} can be handled using the equivalent depth and porosity corrections in Fig. 4.

time-deformation trends will have been monitored in the case of many of the larger excavations.

11.4. Reassembly of FC and CC and correlation to other parameters

The five example rock masses, as visualised through their 'frictional' and 'cohesive' components in the two preceding tables, can be 'reassembled' into Q and Q_c values. We can then examine their relation to other properties like V_p, E_{mass} and L to get a feel for the suggested correlations. An important point to remember is of course that the same Q-value can have different combinations of parameters, and different relative magnitudes of FC and CC. This positive aspect is of course also a source of potential error when a single classification rating (Q or RMR or GSI, etc.) is used for design or for correlation to other parameters. However, there is generally a 'drift' of all parameters as conditions change, probably bought about by the historic presence or absence of water (or hydrothermal fluids) in more, or less jointed cases respectively.

11.5. A discussion of 'c' and 'ϕ' for rock masses

Although it is perhaps unwise to present the CC and FC components of Q_c as approximations to 'c' and 'ϕ' for rock masses (since we really hardly know what these values are), it can be concluded that splitting Q_c (or Q_t) into these shear-strength-like components is likely to be more accurate than suggesting fixed 'c' and 'ϕ' values as relevant for a specific Q-class. A suggestion that $Q = 10-100$ has 'c' > 10 MPa and 'ϕ' $> 45^\circ$ may not always be correct. However, these estimates are likely to be more accurate for hard rock than the suggestion in the RMR tables [23], that RMR = 81–100 has 'c' > 0.4 MPa and 'ϕ' $> 45^\circ$. The former, although strictly an inequality, gives the impression of far too low a cohesion for hard rock, and was perhaps estimated from experience of coal measure rocks, from which many RMR case records were derived.

A current, major underground rock mass characterisation project has demonstrated that subsequent rock mass classification methods have tended to 'copy' the sometimes obviously inaccurate (too low) rock class-based estimates of 'c' and 'ϕ' from RMR. There was found to be an inexplicable degree of agreement between the recent classification methods and RMR, concerning 'c' and 'ϕ' for rock masses, possibly because of the scarcity of actual data that was available during the development of some of the 'empirical' predictions.

Unfortunately, 'c' and 'ϕ' are among the most difficult parameters to assess or measure in rock mechanics, and of course they are usually anisotropic and stress-dependent properties. In addition, a given RMR value, or other classification rating like GSI or RMi, should not be expected to give a unique pair of 'c' and 'ϕ' values. The details of the rock mass structure, and the strength of individual joint sets or discontinuities, will tend to determine the relative magnitudes of 'c' and 'ϕ', and the extent to which they are isotropic or anisotropic. Furthermore, RMR and GSI have very small numerical ranges with which to describe the multitude of potential rock mass characteristics. The same criticism must be levelled at Q, but it is perhaps some five orders-of-magnitude closer to the geohydrologic diversity we try to model, if we assume that the usual range of RMR and GSI is about 5–100.

Inevitably, the relative ease of continuum modelling has caused a disproportionate number of errors in modeller's assessments of rock mass parameters, and the results of such modelling may sometimes bear little relation to commonly observed behaviour. The desirable extension of a global Mohr–Coulomb 'c' and 'ϕ' criterion to a non-linear Hoek-Brown strength criterion still leaves anisotropy unsolved, and an accepted criterion for representing block rotation modes apparently remains as a distant goal in continuum modelling.

It is strongly suspected that a low CC value and a disproportionally high FC value may stimulate a rotational mode of failure, due to joint strength scale effects [7] and due to the block corner interaction

problem. A large scale of loading in relation to a small scale of block size (i.e. a low RQD/J_n ratio) seems to stimulate this mode of deformation or failure, as evidenced by physical models of discontinua [28], distinct element modelling with small block sizes, [40] and most important of all, real large scale deformations and failures of jointed rock masses. *Independent* values of friction and cohesion may be needed to identify, and then to provide input for the future solution of this important continuum modelling problem.

11.6. Tunnelling conditions relevant to the example cases 1–5

With reference to Table 6, it is pertinent to consider the *Q*-system support recommendations for the five simulated rock masses. Fig. 1 shows that a 10 m span road tunnel (with ESR = 1.0) could remain without support when $Q = 100$ (case #1), at least when following typical NMT philosophy. The characteristics of this rock mass satisfy all the criteria of permanently unsupported excavations [41]. It has only one joint set, which has a dilatant character, and there is no water.

All the other cases lie within the fair, poor, very poor and exceptionally poor rock mass categories. Case #2 has too many degrees of freedom for block fall-out despite reasonable frictional strength, so requires at least a 4 cm layer of shotcrete and systematic bolting, c/c 2.4 m. Case #3 will probably give a lot of overbreak and needs more support and reinforcement, and case #4 will likely create a significant delay in tunnelling progress due to the need for heavy B + S(fr) support, probably with rib reinforced shotcrete arches (RRS).

Case #5 may be equivalent to a major fault zone which will require drainage, pre-injection and spiling—perhaps even a pipe-roof—in fact improvements to the abysmally poor existing rock–soil–water characteristics. In the absence of this, a TBM would be stuck for months, and a drill-and-blast or back-hoe digging of this zone would likely be *preceded* by a massive collapse, also taking perhaps a month or more to solve, using the inevitably less effective, post-collapse measures that tend to be extremely labour intensive.

It is easy to speculate that an even lower J_w value in case #5 (e.g. 0.05) would cause a piping failure, filling the tunnel with water, rock and clay, and probably terminating in a very low angle debris fan some distance from the previous tunnel face. There are several cases where tunnels have been filled with rock and clay for 100 m or more, occasionally with tragic loss of life, and sometimes with serious water flooding perhaps reaching kilometres. The initial water pressure and volume of storage, combined with the initial permeability and its coupling with tunnel deformation effects are all determinant factors, besides the susceptibility to low 'c' and 'ϕ' (or CC and FC) in sheared, fragmented rock and clay masses. This is an appropriate point to introduce the final topic of pre-grouting, which will be demonstrated to have positive effects on the tunnelling that reach much wider than water control alone.

12. *Q*-parameter interpretation of potential pre-grouting effects

Modern pre-grouting, using the combined advantages of computer-steered drill jumbos, high pressure injection equipment, micro and ultrafine cements in micro-silica suspensions of cigarette-smoke-sized 0.15 mm particles (perhaps with timed setting of an outer or inner blocker grout), are capable of solving many instability and leakage problems in tunnelling. 'Strengthening the case for grouting' is a fitting title of a recent article addressing the additional strengthening effects of grouting on the rock mass, besides water control.

12.1. Permeability tensor principal value rotation

An important clue to the subject of rock mass property improvement by grouting was provided some years ago in Brazil, when IPT of Sao Paulo were monitoring the effect of dam abutment grouting [42]. The unusual three-dimensional hydrotomography test equipment and test principles are illustrated at the top of Fig. 13. Three boreholes—SR-A1, A6 and D6 were water flow tested as a group before grouting. Three new holes—SR-I, -II and -III were drilled close by, and flow tested as a group, after normal-Portland cement grouting of the first three holes.

Conventional, single-hole, equivalent porous medium interpretation of the grouting effect on the water permeability is shown as depth logs in Fig. 13 (bottom left). A reduction of permeability of 10^{-1}–10^{-3} m/s is indicated, which was to be expected, in view of the original high permeability of 10^{-3}–10^{-5} m/s, despite the maximum 100–140 μm particle sizes of the normal Portland cement. Current opinion is that physical joint apertures (E) down to about 0.4 mm can be grouted with such cement—but the hydraulic apertures (e) would usually be less than this due to roughness JRC, and due to the usually tortuous flow paths within interlocking rock joints [43].

The important result for rock-mass-improvement-by-grouting interpretation, is the unconventional and unfortunately rare recording of the three-dimensional penetration effects of grout, which here gave a 17-fold reduction and roughly a 66° rotation of the K_{max} direction, and a 12-fold reduction and roughly a 148° rotation of the K_{min} direction. By implication, the most permeable (and perhaps least normal-stressed) joint set was successfully grouted, and presumably, even the least

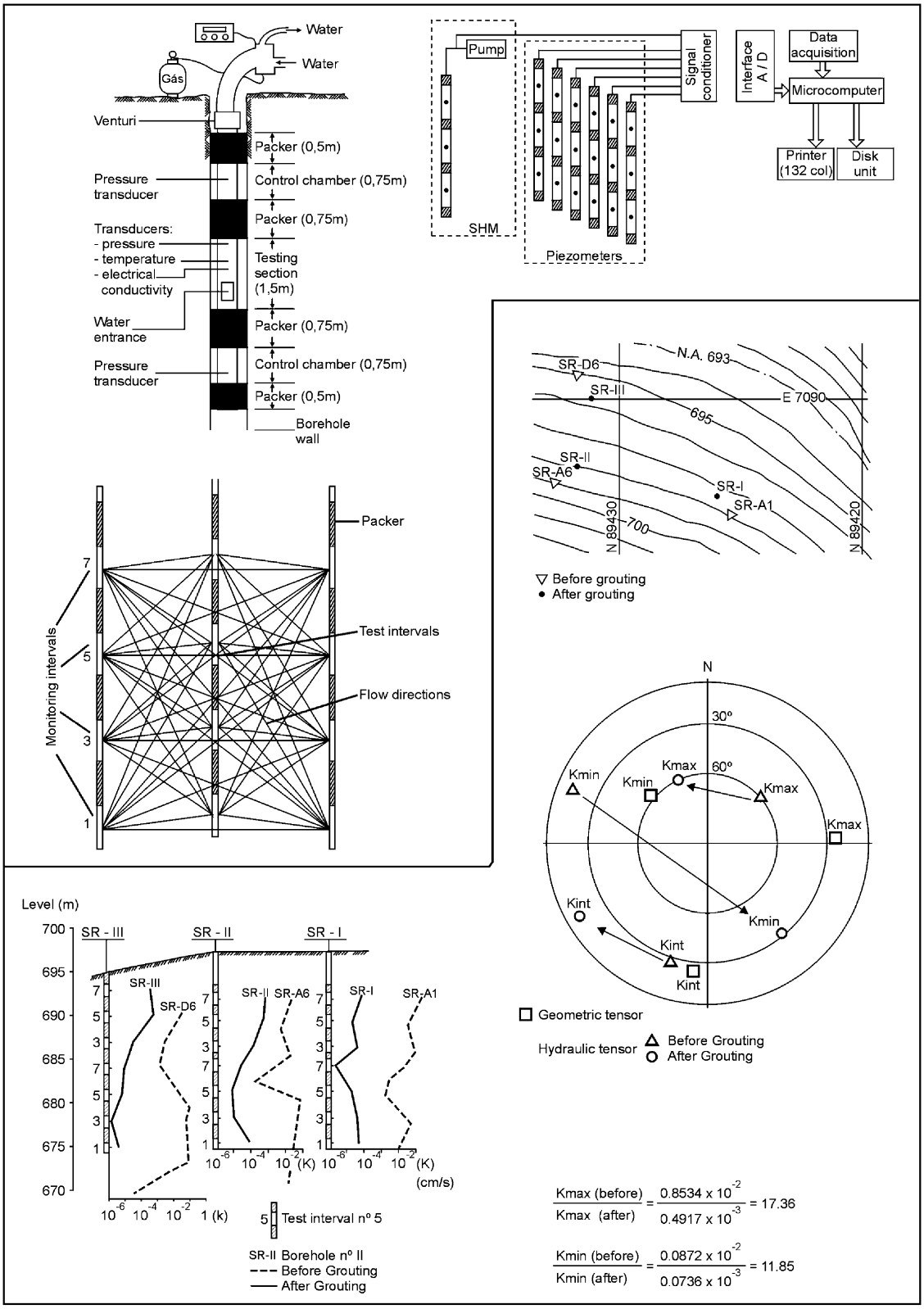

Fig. 13. Multiple-packer, multiple-borehole, 3D-hydrotomography testing by IPT Sao Paulo, of dam foundation permeabilities before-and-after grouting. Permeability principal value rotation (and magnitude reduction) due to sealing of the most permeable joint sets is indicated [42].

permeable set was much improved. There was also fair correlation of the results with the geometric tensors that were derived from joint set orientations and IPTs estimation of the average hydraulic apertures [42]. This rotation of principal directions of the permeability tensors, and the 'homogenization' effect, justifies the potential Q-parameter improvements that are discussed below, following [2,44].

12.2. Particle size and joint aperture limits in grouting

Obviously there are many tunnels that require strict water control, and correspondingly few litres of inflow per minute per 100 m of tunnel to avoid environmental problems such as differential building settlement above over-lying clays. To achieve only 1 Lugeon or roughly 10^{-7} m/s appears to be possible with cement particles of maximum 100–140 μm size. Microfine and ultrafine cements with maximum particle sizes as small as 30 and 15 μm, make it possible to grout down to physical apertures (E) of about 0.1 and 0.05 μm respectively, using the 3 or $4 \times D_{max}$ rule-of-thumb, for which there is some laboratory test evidence [45]. Since there is an increasing ratio of the joint apertures E/e as E, the physical aperture reduces (or stress increases), even smaller permeabilities can be reached with state-of-the-art pre-grouting.

Today it is apparently possible to achieve slightly better than 10^{-8} m/s with systematic pre-grouting, which might be equivalent to about $5\,\ell$/min/100 m in a typical tunnelling project. The result depends of course on tunnel depth below groundwater level, and tunnel size will also play a role in the modified radial flow equations for flow from beneath an equipotential.

A detailed discussion of the possible improvements to the six Q-parameters that may be achieved by systematic pre-injection using the new multi-grout concepts recently applied in Norway, has been given elsewhere [44]. The over-riding assumption is that the grout will follow the paths of least resistance both as regards initial permeability and grout-pressure-modified permeability. The most permeable and least normal-stressed joint set should figure prominently, and may give the permeability principal value rotation and reduction in magnitude, as identified in Fig. 13. Often, this most permeable and most easily injected joint set will also have qualified for the pre-grouting J_r/J_a rating, so this ratio may be changed due to the grouting, and result in an even better result.

12.3. Improving Q-parameter ratings through pre-grouting

The following small changes to the six Q-parameters can be envisaged with the set of initial rock mass conditions assumed here. Lesser or greater improvements due to pre-injection will occur in other cases, as discussed in [44].

We will assume that in a certain rock mass, pre-grouting may cause moderate, individual effects like the following:

RQD increases e.g. 30–50%, J_n reduces e.g. 9–6, J_r increases e.g. 1–2 (due to sealing of most of set #1), J_a reduces e.g. 2 to 1 (due to sealing of most of set #1), J_w increases e.g. 0.5–1 (even with $J_w = 1$, tunnel ventilation air may contain moisture), SRF (might increase in faulted rock with little clay, or if near-surface).

$$\text{Before pre-grouting} \quad Q = \frac{30}{9} \times \frac{1}{2} \times \frac{0.5}{1} = 0.8.$$

$$\text{After pre-grouting} \quad Q = \frac{50}{6} \times \frac{2}{1} \times \frac{1}{1} = 17.$$

12.4. Improving rock mass properties through pre-grouting

We can now use the Q-correlation equations developed earlier to predict typical, but perhaps even conservative estimates of the potentially improved rock mass properties and tunnelling characteristics. We will assume $\sigma_c = 50$ MPa and that the tunnel has a 10 m span, with a required safety level of ESR = 1.0 (for a main road tunnel) [3,5]. See Table 7 for results.

The most surprising and largest predicted improvements in properties and tunnelling conditions are undoubtedly FC—the frictional component of the previously least favourable and most permeable joint set, and Δ—the deformation.

When interpreting the magnitude of so many potential improvements due to successful grouting, it is important to emphasise the 'homogenization' (and reduction) of the permeability tensors that have been measured following successful grouting [42]. An additional effect not included in Table 7 is the likely consolidation or stress homogenization and *increase of stress* caused by forced penetration of grout several or many metres into the rock mass, perhaps with pressures as high as 9 or 10 MPa when rock mass conditions and depth allows this.

According to the 'stressed' velocity and modulus model shown in Fig. 4, this high pressure injection will cause a certain stiffening of the rock mass above and beyond that modelled in the example given in Table 7. However at depths of hundreds of metres, an injection pressure of 9 or 10 MPa will have relatively less influence on the local state of stress, unless there is unusually high stress anisotropy and a low σ_h minimum component, as within a normal faulted terrain, where permeabilities may be very high-even at considerable depth.

Table 7
An example of rock mass and tunnelling improvements that might be achieved by pre-injection with state-of-the-art, fine, cementicious multi-grouts in a typical rock mass of rather poor quality

Before pre-grouting	After pre-grouting	See equation or figure
$Q = 0.8$ (very poor)	$Q = 16.7$ (good)	
$Q_c = 0.4$	$Q_c = 8.3$	3
$V_p = 3.1$ km/s	$V_p = 4.4$ km/s	4 (near surface, $n = 1\%$)
$E_{mass} = 7$ GPa	$E_{mass} = 20$ GPa	9 (near surface, $n = 1\%$)
$Sigma_{cm} = 9$ MPa	$Sigma_{cm} = 25$ MPa	13 (assume $\gamma = 2.5$ t/m^3)
$P_r = 13.6$ t/m^2	$P_r = 4.9$ t/m^2	16 (MPa to t/m^2)
$L = 2.5$	$L = 0.1$	18
$K = 2.5 \times 10^{-7}$ m/s	$K = 10^{-8}$ m/s	(assume $1L = 10^{-7}$ m/s)
$\Delta = 25$ mm	$\Delta = 1$ mm	19
FC = 14°	FC = 63°	23
CC = 1.7 MPa	CC = 8.3 MPa	24
B 1.6 m c/c	B 2.4 m c/c	Fig. 1 (Q-support chart)
S(fr) 10 cm	None	Fig. 1 (Q-support chart)

13. Conclusions

1. The traditional use of the Q-system for rock mass *classification* and empirical design of rock reinforcement and tunnel support has been extended in several ways in this paper. Key rock mass properties and tunnel behaviour characteristics that are strongly related to the six-order-of-magnitude Q-value are estimated, and their potential interactions have been explored. The appendix contains all the traditional Q-parameter ratings for *classification* of rock mass conditions and support needs caused by underground excavation. In addition there are new footnotes for advising on suitable choices of existing parameter ratings when basic rock mass *characterisation* is to be performed, away from the influence of any excavation.
2. It is concluded that the broad, six-order of magnitude Q-value scale, and the even broader nine-order of magnitude Q_c-value scale, give relatively simple correlations with parameters needed for design, due to the fact that rock masses also display a huge range of strengths, stiffnesses and degrees of stability or instability. An RMR or GSI scale of only about 10–100, i.e. one order of magnitude, cannot easily correlate with phenomena as different for instance, as the landmark Sugarloaf Mountain of Rio de Janeiro, where Q may approach 1000, or piping failure causing a tunnel to fill with 7000 m^3 of clay-bearing quartzite (and much greater volumes of water). Here, Q may have approached a limit of 0.001, until J_w improved due to relief of some of the extreme water pressure.
3. Seismic P-wave velocity V_p, and static modulus of deformation E_{mass} can clearly be linked, due to their individual relationship with the Q-value, which has been normalised by consideration of uniaxial compression strengths different from 100 MPa. The resulting Q_c-value is reduced or increased in proportion to σ_c, which removes the need for 'mobilisation' of σ_c through the strength to stress ratio found in SRF. A potential linkage of the high pressure and therefore deforming Lugeon test value with Q_c has also been identified, and a theoretical basis for this has been discussed, assuming an absence of clay in the joints.
4. The strong effects of depth or stress level on V_p and E_{mass}, and their anisotropy when jointing and/or stresses are anisotropic, has been emphasised. The use of an oriented Q and Q_c value has therefore been proposed, using an oriented RQD_0, and a J_r/J_a ratio relevant to the loading or measurement direction. An estimate of rock mass compressive strength developed for the Q_{TBM} model that allows for matrix anisotropy has been reproduced. This is based on the increased ratio of σ_c/I_{50} for foliated and schistose rocks, which may easily reach 75 or more in slates, or about a three-fold increase compared to more isotropic rocks.
5. Support pressure P_r and the static modulus of deformation E_{mass} are found to be inversely related, due to their inverted empirical relations to the Q-value. The additional trend for inverse proportionality between tunnel deformation and Q-value, and between Lugeon value and the Q or Q_c value, actually means that tunnel deformation and typically recorded Lugeon values may have a special relationship, since deformation in millimetres would be implied to very roughly equal the span in metres multiplied by the Lugeon value, with the scatter of data not forgotten. This *perhaps* helps to explain the very beneficial effect of pre-grouting on tunnel stability, which gives many predictable improvements to the properties of the rock mass, besides water control.
6. The various possible effects of pre-grouting have been investigated in an example rock mass, having specific Q-parameters before grouting, with small improvements of most Q-parameters as a result of the grouting. Three-dimensional hydrotomography from a Brazilian dam abutment, showing rotation and reduction of the principal values of permeability, with general homogenization caused by grouting, have been used to justify some of the Q-parameter improvements. These assumed improvements are based on the concept of preferential grouting of the most permeable and least favourable joint set. However, when clay is present the minimum J_r/J_a ratio may not correspond to the direction of highest permeability, and less benefit from the grouting may be achieved, as indeed experienced in practice.
7. The seven Q_c-parameters have been "re-assembled" as two components instead of three, to derive

estimates of the potential frictional component FC, which is like an effective friction angle, and the cohesive component CC, which resembles the cohesion of a rock mass. The latter is related to block size and the degrees of freedom for movement, given largely by J_n. By implication, the original Q-value that was derived from case records of rock bolt and shotcrete tunnel support needs, consists approximately of the product of effective friction coefficient and cohesive strength. Clearly this is a powerful prescription of the need for rock reinforcement and support, when radial stress has been reduced virtually to zero by tunnel or cavern excavation. One may now speculate that the units of Q resemble MPa, more accurately so since the normalisation of Q with $\sigma_c/100$.

8. There will be a tendency for fairly low values of CC, and for fairly high values of FC, to favour rotational modes of deformation and failure, when the overstressed area or volume is large, compared to the typical block size. An accepted constitutive model to represent rotational failure modes for use in continuum approximations is overdue, since rotation occurs in physical and numerical models of discontinua, and obviously in some large, natural and engineered rock slopes.

Appendix A. Q-method of rock mass classification

(1) The following tables (see Tables A1–A6) contain all the ratings necessary for *classifying* the Q-value of a rock mass. The ratings form the basis for the Q, Q_c and Q_0 estimates of rock mass quality (Q_c needing only multiplication of Q by $\sigma_c/100$, and Q_0 the use of a specifically oriented RQD, termed RQD_0 relevant to a loading or measurement direction). All the *classification* ratings needed for tunnel and cavern design are given in the six tables, where Q only would usually apply.

(2) For correlation to engineering parameters as described in this paper, use Q_c (multiplication of Q by $\sigma_c/100$). For specific loading or measurement directions in anisotropically jointed rock masses use RQD_0 in place of RQD in the Q estimate. This means that an *oriented* Q_c value should contain a correctly *oriented* RQD_0 for better correlation to *oriented* engineering parameters.

(3) Q-parameters are most conveniently collected using *histogram logging* as shown in [25]. A specially prepared logging sheet is shown in Fig. 14. Besides space for recording the usual variability of parameters, for structural domains 1 and 2, etc., it contains reminders of the tabulated ratings at the base of each histogram. Space for presentation of results for selected (or all) domains at the top of the diagram, includes *typical range, weighted mean and most frequent* (Q-parameters, and Q-values).

(4) During field logging, allocate running numbers to the structural domains, or core boxes, or tunnel sections, e.g. 1 = D1, 2 = D2, etc. and write the numbers in the allotted histogram columns, using a regular spacing for each observation such as 11, 113, 2245, 6689, etc. In this way the histograms will give the correct visual frequency of all the assembled observations, in each histogram column. Besides this, it will be easy to find the relevant Q-parameters for a particular domain, core box or section of tunnel, for separate analysis and reporting. Overall frequencies of observations of each rating (or selected sets of data) can be given as numbers on separate logging sheets. Large data sets can be computerised when returning from the field.

(5) It is convenient and correct to record rock mass variability. Therefore allow as many as *five* observations of each parameter, for instance in a 10 m length of tunnel. If all observations are the same, great uniformity of character is implied, if variable—this is important information. At 'the end of the day' the histograms will give a correct record of variability, or otherwise.

(6) Remember that logged RQD of < 10, including 0, are set to a nominal 10 when calculating Q. In view of the log scale of Q, the histograms of RQD in the logging sheet will be sufficiently accurate if given mean values, from left to right, of 10, 15, 25, 35……85, 95, 100. The log scale of Q also suggests that decimal places should be used sparingly. The following is considered realistic 0.004, 0.07, 0.3, 6.7, 27, 240. Never report that $Q =$ 6.73 or similar, since a false sense of accuracy will be given.

(7) Footnotes below the tables that follow, also give advice for site *characterisation* ratings for the case of J_w and SRF, which must not be set to 1.0 and 1.0, as some authors have suggested. This destroys the intended multi-purposes of the Q-system, which has an entirely different structure compared to RMR.

Important: Use all appropriate footnotes under the six tables. Some have been updated or added since the minor 1993/1994 updating of three SRF values for highly stressed massive rock, which were changed due to 'new' support techniques, namely B + S(fr) [46].

$$Q = \frac{RQD}{J_n} \times \frac{J_r}{J_a} \times \frac{J_w}{SRF}$$

Table A1

Rock quality designation		RQD (%)
A	Very poor	0–25
B	Poor	25–50
C	Fair	50–75
D	Good	75–90
E	Excellent	90–100

Notes: (i) Where RQD is reported or measured as $\leqslant 10$ (including 0), a nominal value of 10 is used to evaluate Q. (ii) RQD intervals of 5, i.e., 100, 95, 90, etc., are sufficiently accurate.

Table A2

Joint set number		J_n
A	Massive, no or few joints	0.5–1
B	One joint set	2
C	One joint set plus random joints	3
D	Two joint sets	4
E	Two joint sets plus random joints	6
F	Three joint sets	9
G	Three joint sets plus random joints	12
H	Four or more joint sets, random, heavily jointed, 'sugar-cube', etc.	15
J	Crushed rock, earthlike	20

Notes: (i) For tunnel intersections, use $(3.0 \times J_n)$. (ii) For portals use $(2.0 \times J_n)$.

Table A3

Joint roughness number		J_r
(a) *Rock-wall contact, and (b) rock-wall contact before 10 cm sear*		
A	Discontinuous joints	4
B	Rough or irregular, undulating	3
C	Smooth, undulating	2
D	Slickensided, undulating	1.5
E	Rough or irregular, planar	1.5
F	Smooth, planar	1.0
G	Slickensided, planar	0.5
(b) *No rock-wall contact when sheared*		
H	Zone containing clay minerals thick enough to prevent rock-wall contact.	1.0
J	Sandy, gravely or crushed zone thick enough to prevent rock-wall contact	1.0

Notes: (i) Descriptions refer to small-scale features and intermediate scale features, in that order. (ii) Add 1.0 if the mean spacing of the relevant joint set is greater than 3 m. (iii) $J_r = 0.5$ can be used for planar, slickensided joints having lineations, provided the lineations are oriented for minimum strength. (iv) J_r and J_a classification is applied to the joint set or discontinuity that is least favourable for stability both from the point of view of orientation and shear resistance, τ(where $\tau \approx \sigma_n \tan^{-1}(J_r/J_a)$.

Table A4

Joint alteration number		ϕ_r approx. (deg)	J_a
(a) *Rock-wall contact (no mineral fillings, only coatings)*			
A	Tightly healed, hard, non-softening, impermeable filling, i.e., quartz or epidote	—	0.75
B	Unaltered joint walls, surface staining only	25–35	1.0
C	Slightly altered joint walls, non-softening mineral coatings, sandy particles, clay-free disintegrated rock, etc.	25–30	2.0
D	Silty- or sandy-clay coatings, small clay fraction (non-softening)	20–25	3.0
E	Softening or low friction clay mineral coatings, i.e., kaolinite or mica. Also chlorite, talc, gypsum, graphite, etc., and small quantities of swelling clays	8–16	4.0
(b) *Rock-wall contact before 10 cm shear (thin mineral fillings)*			
F	Sandy particles, clay-free disintegrated rock, etc.	25–30	4.0
G	Strongly over-consolidated non-softening clay mineral fillings (continuous, but <5 mm thickness)	16–24	6.0
H	Medium or low over-consolidation, softening, clay mineral fillings (continuous, but <5 mm thickness)	12–16	8.0
J	Swelling-clay fillings, i.e., montmorillonite (continuous, but <5 mm thickness). Value of J_a depends on per cent of swelling clay-size particles, and access to water, etc.	6–12	8–12
(c) *No rock-wall contact when sheared (thick mineral fillings)*			
KLM	Zones or bands of disintegrated or crushed rock and clay (see G, H, J for description of clay condition)	6–24	6, 8, or 8–12
N	Zones or bands of silty- or sandy-clay, small clay fraction (non-softening)	—	5.0
OPR	Thick, continuous zones or bands of clay (see G, H, J for description of clay condition)	6–24	10, 13, or 13–20

Table A5

	Joint water reduction factor	Approx. water pres. (kg/cm^2)	J_w
A	Dry excavations or minor inflow, i.e., <5 l/min locally	<1	1.0
B	Medium inflow or pressure, occasional outwash of joint fillings	1–2.5	0.66
C	Large inflow or high pressure in competent rock with unfilled joints	2.5–10	0.5
D	Large inflow or high pressure, considerable outwash of joint fillings	2.5–10	0.33
E	Exceptionally high inflow or water pressure at blasting, decaying with time	>10	0.2–0.1
F	Exceptionally high inflow or water pressure continuing without noticeable decay	>10	0.1–0.05

Notes: (i) Factors C to F are crude estimates. Increase J_w if drainage measures are installed. (ii) Special problems caused by ice formation are not considered. (iii) For general characterisation of rock masses distant from excavation influences, the use of $J_w = 1.0$, 0.66, 0.5, 0.33, etc. as depth increases from say 0–5, 5–25, 25–250 to >250 m is recommended, assuming that RQD/J_n is low enough (e.g. 0.5–25) for good hydraulic connectivity. This will help to adjust Q for some of the effective stress and water softening effects, in combination with appropriate characterisation values of SRF. Correlations with depth-dependent static deformation modulus and seismic velocity will then follow the practice used when these were developed.

Table A6

Stress reduction factor		SRF		
(a) *Weakness zones intersecting excavation, which may cause loosening of rock mass when tunnel is excavated*				
A	Multiple occurrences of weakness zones containing clay or chemically disintegrated rock, very loose surrounding rock (any depth)	10		
B	Single weakness zones containing clay or chemically disintegrated rock (depth of excavation $\leqslant 50$ m)	5		
C	Single weakness zones containing clay or chemically disintegrated rock (depth of excavation >50 m)	2.5		
D	Multiple shear zones in competent rock (clay-free), loose surrounding rock (any depth)	7.5		
E	Single shear zones in competent rock (clay-free), (depth of excavation $\leqslant 50$ m)	5.0		
F	Single shear zones in competent rock (clay-free), (depth of excavation >50 m)	2.5		
G	Loose, open joints, heavily jointed or 'sugar cube', etc. (any depth)	5.0		
		σ_c/σ_1	σ_θ/σ_c	SRF
(b) *Competent rock, rock stress problems*				
H	Low stress, near surface, open joints	>200	<0.01	2.5
J	Medium stress, favourable stress condition	200–10	0.01–0.3	1
K	High stress, very tight structure. Usually favourable to stability, may be unfavourable for wall stability	10–5	0.3–0.4	0.5–2
L	Moderate slabbing after >1 h in massive rock	5–3	0.5–0.65	5–50
M	Slabbing and rock burst after a few minutes in massive rock	3–2	0.65–1	50–200
N	Heavy rock burst (strain-burst) and immediate dynamic deformations in massive rock	<2	>1	200–400
		σ_θ/σ_c	SRF	
(c) *Squeezing rock: plastic flow of incompetent rock under the influence of high rock pressure*				
O	Mild squeezing rock pressure	1–5	5–10	
P	Heavy squeezing rock pressure	>5	10–20	
		SRF		
(d) *Swelling rock: chemical swelling activity depending on presence of water*				
R	Mild swelling rock pressure	5–10		
S	Heavy swelling rock pressure	10–15		

Notes: (i) Reduce these values of SRF by 25–50% if the relevant shear zones only influence but do not intersect the excavation. This will also be relevant for characterisation. (ii) For strongly anisotropic virgin stress field (if measured): When $5 \leqslant \sigma_1/\sigma_3 \leqslant 10$, reduce σ_c to $0.75\sigma_c$. When $\sigma_1/\sigma_3 > 10$, reduce σ_c to $0.5\sigma_c$, where σ_c is the unconfined compression strength, σ_1 and σ_3 are the major and minor principal stresses, and σ_θ the maximum tangential stress (estimated from elastic theory). (iii) Few case records available where depth of crown below surface is less than span width, suggest an SRF increase from 2.5 to 5 for such cases (see H). (iv) Cases L, M, and N are usually most relevant for support design of deep tunnel excavations in hard massive rock masses, with RQD/J_n ratios from about 50–200. (v) For general characterisation of rock masses distant from excavation influences, the use of SRF = 5, 2.5, 1.0, and 0.5 is recommended as depth increases from say 0–5, 5–25, 25–250 to >250 m. This will help to adjust Q for some of the effective stress effects, in combination with appropriate characterisation values of J_w. Correlations with depth-dependent static deformation modulus and seismic velocity will then follow the practice used when these were developed. (vi) Cases of squeezing rock may occur for depth $H > 350Q^{1/3}$ according to Singh [34]. Rock mass compression strength can be estimated from $\mathrm{SIGMA_{cm}} \approx 5\gamma Q_c^{1/3}$ (MPa) where γ is the rock density in t/m^3, and $Q_c = Q \times \sigma_c/100$, Barton [29].

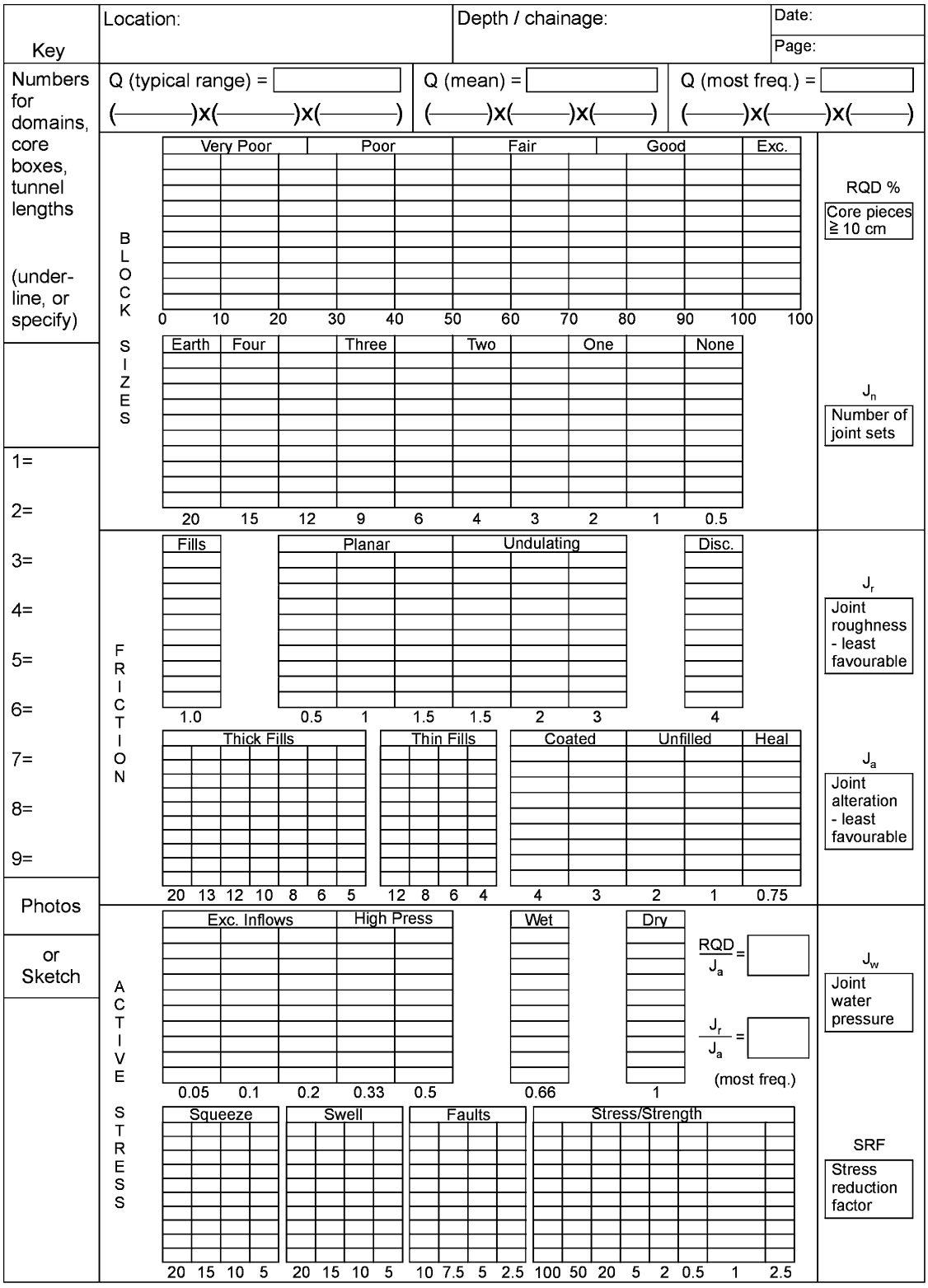

Fig. 14. Field logging sheet for recording the statistics of all Q-parameter observations can be used for field mapping of surface exposures, core logging or underground excavation logging. Note that almost all of the ratings are given at the base of each column.

References

[1] Deere DU, Hendron AJ, Patton FD, Cording EJ. Design of surface and near-surface construction in rock. In: Fairhurst C, editor. Proceedings of the US Rock Mechanics Symposium, Failure and Breakage of Rock. New York: Society of Mining Engineers of AIME, 1967. p. 237–302.

[2] Barton N. General Report concerning some 20th Century lessons and 21st Century challenges in applied rock mechanics, safety and control of the environment. Proceedings of the 9th Congress of ISRM, Paris, Gen. Rept. Session 1, vol. 3. Rotterdam, Balkema, 1999.

[3] Barton N, Lien R, Lunde J. Engineering classification of rockmasses for the design of tunnel support. Rock Mech 1974;6(4):189–236.

[4] Barton N. Rock mass classification, tunnel reinforcement selection using the *Q*-system. Proceedings of the ASTM Symposium on Rock Classification Systems for Engineering Purposes. Cincinnati, Ohio, 1987.

[5] Grimstad E, Barton N. Updating of the Q-system for NMT. In: Kompen, Opsahl, Berg, editors. Proceedings of the International Symposium on Sprayed Concrete—Modern Use of Wet Mix Sprayed Concrete for Underground Support, Fagernes. Oslo: Norwegian Concrete Association, 1993.

[6] Barton N, By TL, Chryssanthakis P, Tunbridge L, Kristiansen J, Løset F, Bhasin RK, Westerdahl H, Vik G. Predicted and measured performance of the 62 m span Norwegian olympic ice hockey Cavern at Gjøvik. Int J Rock Mech, Min Sci Geomech Abstr 1994;31(6):617–41.

[7] Barton N, Bandis S, Bakhtar K. Strength, deformation and conductivity coupling of rock joints. Int J Rock Mech Min Sci Geomech Abstr 1985;22(3):121–40.

[8] Barton N. Geotechnical Design. World Tunnelling, November 1991, p. 410–6.

[9] Sjøgren B, Øfsthus A, Sandberg J. Seismic classification of rock mass qualities. Geophys Prospecting 1979;27:409–42.

[10] Denekamp S. Personal communication, 1992.

[11] Barton N. The influence of joint properties in modelling jointed rock masses. Keynote Lecture, 8th Congress of ISRM, Tokyo, vol. 3. Rotterdam: Balkema, 1995.

[12] Barton N. Seismic velocity and rock quality. Text book, in preparation.

[13] Hudson JA, Jones EJW, New BM. P-wave velocity measurements in a machine-bored, chalk tunnel. Q J Eng Geol 1980;13:33–43.

[14] New B. Personal communication, 1992.

[15] Cosma C, Olsson O, Keskinen J, Heikkinen P. Seismic characterization of fracturing at the Äspö Hard Rock Laboratory, Sweden, from the kilometre scale to the meter scale. Int J Rock Mech Min Sci 2001;38:859–65, Special Issue, Application of Geophysics to Rock Engineering, Pergamon, Elsevier Science Ltd.

[16] Emsley SJ, Olsson O, Stanfors R, Stenberg L, Cosma C, Tunbridge L. Integrated characterisation of a rock volume at the Äspö HRL utilised for an EDZ experiment. In: Barla, editor. Eurock, vol. 2. Rottterdam: Balkema, 1996. p. 1329–36.

[17] Barton N, Løset F, Lien R, Lunde J. Application of the Q-system in design decisions concerning dimensions and appropriate support for underground installations. Int Conf Subsurface Space, Rockstore, Stockholm, Sub-surface Space 1980; 2:553–61.

[18] Chryssanthakis P, Barton N. Predicting performance of the 62 m span ice hockey cavern in Gjøvik, Norway. Proceedings of the International Conference Fractured and Jointed Rock Masses. Lake Tahoe, CA, 1992.

[19] Bieniawski ZT. Determining rock mass deformability: experience from case histories. Int J Rock Mech Min Sci Geomech Abstr 1978;15:237–47.

[20] Serafim JL, Pereira JP. Considerations of the geomechanics classification of Bieniawski. Proceedings of the International Symposium Eng. Geology and Underground Construction. LNEC, Lisbon, 1983. p. 1. II-33–II-42.

[21] Barton N. Estimating rock mass deformation modulus for excavation disturbed zone studies. International Conference on Deep Geological Disposal of Radioactive Waste, Winnepeg, EDZ workshop. Canadian Nuclear Society, 1996. p. 133–44.

[22] Bandis S, Lumsden AC, Barton N. Fundamentals of rock joint deformation. Int J Rock Mech Min Sci Geomech Abstr 1983;20(6):249–68.

[23] Bieniawski ZT. Engineering rock mass classifications: a complete manual for engineers and geologists in mining, civil and petroleum engineering. NewYork: Wiley, 1989, 251p.

[24] Barton N, Bakhtar K. Instrumentation and analysis of a deep shaft in quartzite. Proceedings of the 24th US Symposium on Rock Mechanics. Texas A&M University, Publ. Assoc. of Eng. Geologists, 1983. p. 371–84.

[25] Barton N, Løset F, Smallwood A, Vik G, Rawlings C, Chryssanthakis P, Hansteen H, Ireland T. Geotechnical core characterisation for the UK radioactive waste repository design. Proceedings. of the ISRM Symposium EUROCK. Chester, UK, 1992.

[26] Tanimoto C. Personal communication, 1983.

[27] Addis MA, Barton N, Bandis SC, Henry JP. Laboratory studies on the stability of vertical and deviated boreholes'. Proceedings of the 65th Annual Technical Conference and Exhibition of the Society of Petroleum Engineers. New Orleans, 1990.

[28] Barton N, Hansteen H. Very large span openings at shallow depth: deformation magnitudes from jointed models and F.E. analysis. In: Maevis AC, Hustrulid WA, editors. Proceedings of the Fourth Rapid Excavation and Tunnelling Conference, Atlanta, Georgia, vol. 2. Publ. American Institute of Mining, Metallurgical, and Petroleum Engineers, Inc. New York, 1979. p. 1131–1353.

[29] Barton N. TBM tunnelling in jointed and faulted rock. Rotterdam: Balkema, 2000, 173p.

[30] Quadros EF, Correa Filho D, Azevedo AA. 3-D hydraulic tests for the subway of São Paulo, Brazil, under the Pinheiros River. Proceedings of the 9th Congress of ISRM, Paris, France. Rotterdam: Balkema, 1999. p. 817–23.

[31] Oda M, Yamabe T, Kamemura K. A crack tensor and its relation to wave velocity anisotropy in jointed rock masses. Int J Rock Mech Min Sci 1986;23(6):387–97.

[32] Nunn KR, Barker RD, Bamford D. In situ seismic and electrical measurements of fracture anisotropy in the Lincolnshire Chalk. Q J Eng Geol 1983;16:187–95.

[33] Oberti G, Carabelli E, Goffi L, Rossi PP. Study of an orthotropic rock mass: experimental techniques, comparative analysis of results. Proceedings of the Fourth ISRM Congress, Montreux, vol. 2. Rotterdam: Balkema, 1979. p. 485–91.

[34] Singh B. Norwegian method of tunnelling workshop. New Dehli: CSMRS.

[35] Barton N. A Q-system case record of cavern design in faulted rock. Proceedings of the Fifth International Rock Mechanics and Rock Engineering Conference, Tunnelling in Difficult Conditions. Torino, Italy, 1994. p. 16.1–16.14.

[36] Comité National Français. La deformabilité des massifs rocheux. Analyse et comparaison des resultats. International Congress on Large Dams, vol. 8. Edinburg. Paris: ICOLD, V.1, Q. 28, 1964. p. 287–99.

[37] Chen CN, Guo GC. Rock mass classification and guideline for tunnel convergence. J Chin Inst Civil Hydraulic Eng, Taiwan 1997;9(3):359–67 ((in Chinese)).

[38] Bhasin R, Barton N, Grimstad E, Chryssanthakis P, Shende FP. Comparison of predicted and measured performance of a large

cavern in the Himalayas. Int J Rock Mech Min Sci Geomech Abstr 1996;6:607–26.
[39] Fong C. Personal communication, 2001.
[40] Shen B, Barton N. The disturbed zone around tunnels in jointed rock masses. Int J Rock Mech Min Sci 1997;34(1):117–25.
[41] Barton N. Unsupported underground openings. Rock Mechanics Discussion Meeting, BeFo. Swedish Rock Mechanics Research Foundation, Stockholm, 1976. p. 61–94.
[42] Quadros EF, Correa Filho D. Grouting efficiency using directional (3-D) hydraulic tests in Pirapora Dam, Brazil. In: Fujii, editor. Proceedings of the 8th ISRM congress, Tokyo, 1995. p. 823–6.
[43] Barton N, Quadros EF. Joint aperture and roughness in the prediction of flow and groutability of rock masses. In: Kim K, editor. Proceedings of the NY Rocks'97. 'Linking Science to Rock Engineering. Int J Rock Mech Mining Sci 1997;34(3–4): 907–16.
[44] Barton N, Buen B, Roald S. Strengthening the case for grouting. Tunnels and Tunnelling International, December 2001, January 2002.
[45] Bhasin RK, Johansen PM, Barton N, Makurat A. Rock joint sealing experiments using an ultra fine cement grout. Proceedings of the North American Tunnelling Conference. Seattle, USA, 2002.
[46] Barton N, Grimstad E. The Q-system following 20 years of application in NMT support selection. Proceedings of the 43rd Geomechanic Colloquy, vol. 6. Salzburg, Felsbau, 1994. p. 428–36.